Static, free vibration analyses and dynamic control of composite plates integrated with piezoelectric sensors and...

Article *in* Smart Materials and Structures · August 2013

DOI: 10.1088/0964-1726/22/9/095026

CITATIONS
34

READS
158

4 authors:

Phung-Van Phuc
Ghent University
36 PUBLICATIONS **678** CITATIONS
SEE PROFILE

T. Nguyen-Thoi
Ton Duc Thang University
126 PUBLICATIONS **4,409** CITATIONS
SEE PROFILE

Hoang duc Vinh
University of Technical Education Ho Chi Minh
19 PUBLICATIONS **491** CITATIONS
SEE PROFILE

H. Nguyen-Xuan
Hutech University, Ho Chi Minh City, Vietnam
180 PUBLICATIONS **5,244** CITATIONS
SEE PROFILE

Smart Mater. Struct. **22** (2013) 000000 (17pp) UNCORRECTED PROOF

Static and free vibration analyses and dynamic control of composite plates integrated with piezoelectric sensors and actuators by the cell-based smoothed discrete shear gap method (CS-FEM-DSG3)

(Ed: Editor17)
Ascii/Word/SMS/
sms470236/PAP
Printed 12/8/2013
Spelling US
Issue no
Total pages
First page
Last page
File name
Date req
Artnum
Cover date

Q.1 **P Phung-Van**[1], **T Nguyen-Thoi**[1,2,4], **T Le-Dinh**[3] **and H Nguyen-Xuan**[1,2]

[1] Division of Computational Mechanics, Ton Duc Thang University, Nguyen Huu Tho Street, Tan Phong Ward, District 7, Hochiminh City, Vietnam
[2] Faculty of Mathematics and Computer Science, Department of Mechanics, University of Science, Vietnam National University—HCMC, 227 Nguyen Van Cu, District 5, Hochiminh City, Vietnam
[3] Faculty of Transportation Engineering, HCMC University of Technology, Vietnam National University—HCMC, 268 Ly Thuong Kiet, District 10, Hochiminh City, Vietnam

E-mail: ngttrung@hcmus.edu.vn and thoitrung76@gmail.com

Received 10 April 2013, in final form 24 July 2013
Published
Online at stacks.iop.org/SMS/22/000000

Abstract
The cell-based smoothed discrete shear gap method (CS-FEM-DSG3) using three-node triangular elements was recently proposed to improve the performance of the discrete shear gap method (DSG3) for static and free vibration analyses of isotropic Mindlin plates. In this paper, the CS-FEM-DSG3 is further extended for static and free vibration analyses and dynamic control of composite plates integrated with piezoelectric sensors and actuators. In the piezoelectric composite plates, the electric potential is assumed to be a linear function through the thickness of each piezoelectric sublayer. A displacement and velocity feedback control algorithm is used for active control of the static deflection and the dynamic response of the plates through closed loop control with bonded or embedded distributed piezoelectric sensors and actuators. The accuracy and reliability of the proposed method is verified by comparing its numerical solutions with those of other available numerical results.

Q.2 (Some figures may appear in colour only in the online journal)

1. Introduction

Q.3 The integration of composite plates with piezoelectric materials to give active lightweight smart structures has attracted the considerable interest of researchers in various industries such as automotive sensors, actuators, transducers and active damping devices, etc. Piezoelectric materials are often used to design smart structures in industrial, medical, military and scientific areas. One of the essential features of piezoelectric materials is the ability of transformation between mechanical energy and electric energy. Specifically, when a piezoelectric material is deformed, it generates electric charge, and on the contrary, when an electric field is applied, it will produce mechanical behavior in the structure [1].

[4] Address for correspondence: Faculty of Mathematics and Computer Science, University of Science, Vietnam National University—HCMC, 227 Nguyen Van Cu, District 5, Hochiminh City, Vietnam.

Due to these attractive properties, various numerical methods have been proposed to model and simulate the behavior of piezoelectric composite structures. For static and free vibration analysis, Yang and Lee [2] showed that the early work on structures with piezoelectric layers, which ignored the mass and stiffness of the layers, could lead to substantial errors in the natural frequencies and mode shapes. Pletner and Abramovich [3] studied a consistent technique for modeling piezolaminated shells. Hong and Chopra [4] incorporated the piezoelectric layers as plies with special properties into the laminate and assumed that consistent deformations existed in the substrate and piezoelectric layers. Kim *et al* [5] validated a finite element model of the smart cantilever plate in comparison with experiments. Finite element models for piezoelectric composite beams and plates have been reported in detail in [16–19]. In addition, Liew *et al* [20] applied the element free Galerkin method to laminated composite beams and plates with piezoelectric patches.

For vibration control, analytical methods were initially investigated for smart beams with embedded or surface distributed piezoelectric sensors and actuators [21, 22]. Tzou and Tseng [23] developed a piezoelectric thin hexahedron solid element for analysis of flexible continua plates and shells with distributed piezoelectric sensors and actuators based on brick elements. Kapuria and Yasin [24] proposed active vibration control of smart plates using the directional actuation and sensing capability of piezoelectric composites. Hwang and Park [25], and Lam *et al* [6] reported control algorithms based on classical negative velocity feedback control and the finite element method which were formulated based on the discrete Kirchhoff quadrilateral (DKQ) element or the rectangular plate bending element. Liu *et al* [26, 27] studied active vibration control of beams and plates containing distributed sensors and actuators. In this work, the formulation of the vibration control simulation was based on classical plate theory (CPT) and the radial point interpolation method (RPIM). Also, Wang *et al* [1] studied static shape control for intelligent structures that used a four-node isoparametric element for thin plates. Milazzo and Orlando [28] proposed an equivalent single-layer approach for free vibration analysis of smart laminated thick composite plates. Recently, some finite element formulations for analysis of smart laminated plates and shells were proposed in [29, 30]. So far, to the best of our knowledge, no methods using three-node triangular elements have been developed for analysis of piezoelectric composite plates. This paper will try to fill this gap by using a new three-node triangular plate element proposed recently.

On the other front of the development of numerical methods, Liu and Nguyen-Thoi [31] have integrated the strain smoothing technique into the FEM to create a series of smoothed FEMs (S-FEMs) [32] such as a cell/element-based smoothed FEM (CS-FEM) [33–36], a node-based smoothed FEM (NS-FEM) [37–39], an edge-based smoothed FEM (ES-FEM) [40, 41], a face-based smoothed FEM (FS-FEM) [42] and a group of alpha-FEMs [43–46]. Each of these smoothed FEMs has different properties and has been used to produce desired solutions for a wide class of benchmark and practical mechanics problems. Several theoretical aspects of the S-FEM models have been provided in [47, 48]. The S-FEM models have also been further investigated and applied to various problems such as plates and shells [49–61], piezoelectricity [62], fracture mechanics [63], visco-elastoplasticity [64, 66], limit and shakedown analysis for solids [67–69], and some other applications [70–73], etc.

Among these S-FEM models, the CS-FEM [32, 33] shows some interesting properties in solid mechanics problems. Extending the idea of the CS-FEM to plate structures, Nguyen-Thoi *et al* [74] have recently formulated a cell-based smoothed stabilized discrete shear gap element (CS-FEM-DSG3) using only three-node triangular elements for static and free vibration analyses of isotropic Mindlin plates by incorporating the CS-FEM with the original DSG3 element [75]. In the CS-FEM-DSG3, each triangular element is divided into three sub-triangles, and in each sub-triangle, the stabilized DSG3 is used to compute the strains. Then the strain smoothing technique on the whole triangular element is used to smooth the strains on these three sub-triangles. The numerical results showed that the CS-FEM-DSG3 is free of shear locking and achieves high accuracy compared to exact solutions and other existing elements in the literature.

This paper hence further extends the CS-FEM-DSG3 to static and free vibration analyses and dynamic control of composite plates integrated with piezoelectric sensors and actuators. In the piezoelectric composite plates, the electric potential is assumed to be a linear function through the thickness for each piezoelectric sublayer. A displacement and velocity feedback control algorithm is used for active control of the static deflection and the dynamic response of the plates through closed loop control with bonded or embedded distributed piezoelectric sensors and actuators. The accuracy and reliability of the proposed method will be verified by comparing its numerical solutions with those of other available numerical results.

2. Galerkin weakform and finite element formulation for piezoelectric composite plates

In this section, the Galerkin weakform and finite element formulation for piezoelectric composite plates is established via a variational formulation [9, 10]. Figure 1 shows the geometry of a piezoelectric composite plate. The piezoelectric composite plate is assumed to be perfectly bonded, elastic and orthotropic in behavior [11], with small strains and displacements [12], and the deformation takes place under isothermal conditions. In addition, the piezoelectric sensors/actuators are made of homogeneous and isotropic dielectric materials [13] and high electric fields as well as cyclic fields are not involved [14]. Based on these assumptions, a linear constitutive relationship [8] can be employed for the static and dynamic analysis of the piezoelectric composite plate.

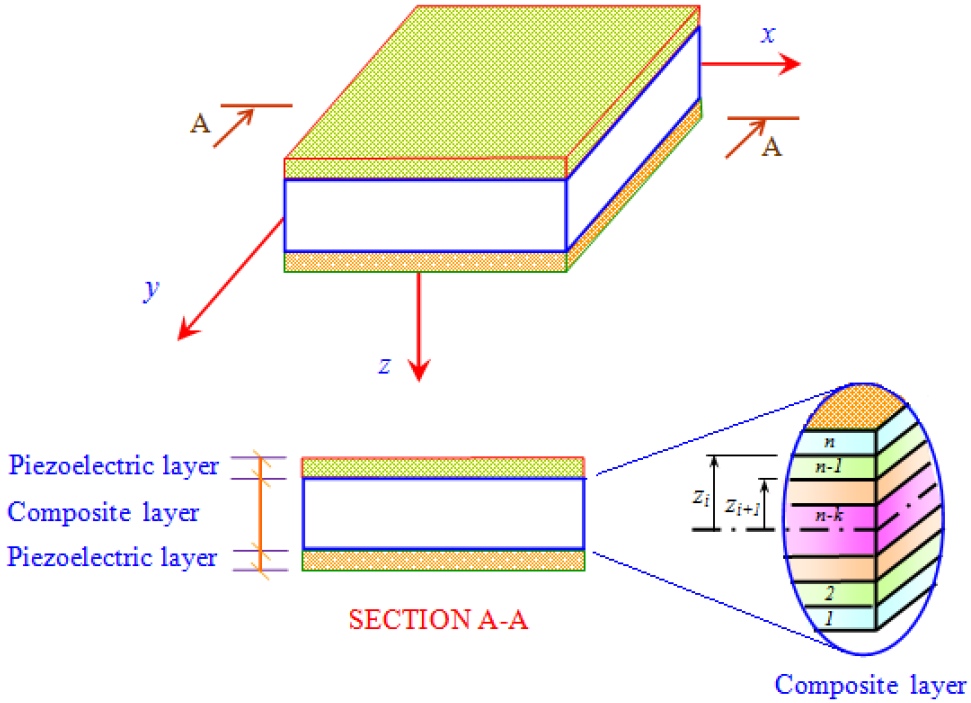

Figure 1. Configuration of a piezoelectric laminated composite plate.

2.1. Linear piezoelectric constitutive equations

The linear piezoelectric constitutive equations can be expressed as

$$\begin{bmatrix} \boldsymbol{\sigma} \\ \mathbf{D} \end{bmatrix} = \begin{bmatrix} \mathbf{c} & -\mathbf{e}^{\mathrm{T}} \\ \mathbf{e} & \mathbf{g} \end{bmatrix} \begin{bmatrix} \boldsymbol{\varepsilon} \\ \mathbf{E} \end{bmatrix} \tag{1}$$

where $\boldsymbol{\sigma}$ and $\boldsymbol{\varepsilon}$ are the stress and strain vectors, $\mathbf{D}$ and $\mathbf{E}$ are the dielectric displacement and electric field vectors, $\mathbf{c}$ is the elasticity matrix displayed in section 2.3.1, $\mathbf{e}$ is the piezoelectric constant matrix and $\mathbf{g}$ denotes the dielectric constant matrix displayed in section 2.4.

In addition, the electric field vector $\mathbf{E}$ is related to the electric potential field ϕ by using a gradient vector [23] as

$$\mathbf{E} = -\mathrm{grad}\,\phi. \tag{2}$$

2.2. Galerkin weakform of the governing equations

The Galerkin weakform of the governing equations of piezoelectric structures can be derived by using Hamilton's variational principle [25] which can be written as

$$\delta L = 0 \tag{3}$$

where L is the general energy functional which describes a summation of kinetic energy, strain energy, dielectric energy and external work and is written in the form of

$$L = \int \left(\tfrac{1}{2}\rho \dot{\mathbf{u}}^{\mathrm{T}}\dot{\mathbf{u}} - \tfrac{1}{2}\boldsymbol{\sigma}^{\mathrm{T}}\boldsymbol{\varepsilon} + \tfrac{1}{2}\mathbf{D}^{\mathrm{T}}\mathbf{E} + \mathbf{u}\mathbf{f}_{\mathrm{s}} - \boldsymbol{\phi}\mathbf{q}_{\mathrm{s}} \right) \mathrm{d}\Omega + \sum \mathbf{u}^{\mathrm{T}}\mathbf{F}_{\mathrm{p}} - \sum \boldsymbol{\phi}\mathbf{Q}_{\mathrm{p}} \tag{4}$$

where $\mathbf{u}$ and $\dot{\mathbf{u}}$ are the mechanical displacement and velocity, $\boldsymbol{\phi}$ is the electric potential, $\mathbf{f}_{\mathrm{s}}$ and $\mathbf{F}_{\mathrm{p}}$ are the mechanical surface loads and point loads, and $\mathbf{q}_{\mathrm{s}}$ and $\mathbf{Q}_{\mathrm{p}}$ are the surface charges and point charges.

In the variational form of equation (3), the mechanical displacement field $\mathbf{u}$ and electric potential field $\boldsymbol{\phi}$ are the unknown functions. To solve these unknowns numerically, it is necessary to use efficient finite element methods to approximate the mechanical displacement field and electric potential field. In this work, the CS-FEM-DSG3 [74] is extended to approximate the mechanical displacement field of composite plates. In addition, due to the above assumptions such that a linear constitutive relationship can be employed [8] for the analysis of the piezoelectric composite plate, the formulation for each field should be presented separately.

2.3. Approximations of the mechanical displacement field

2.3.1. First-order shear deformation theory for a laminated composite plate. Consider a laminated composite plate under bending deformation as shown in figure 2. The middle (neutral) surface of the plate is chosen as the reference plane that occupies a domain $\Omega \subset R^2$. The displacement field according to the Reissner–Mindlin model which is based on the first-order shear deformation theory [76] can be expressed by

$$\begin{aligned} u(x, y, z) &= u_0(x, y) + z\beta_x(x, y) \\ v(x, y, z) &= v_0(x, y) + z\beta_y(x, y) \\ w(x, y, z) &= w(x, y) \end{aligned} \tag{5}$$

where u_0, v_0, w are the displacements of the mid-plane of the plate; β_x, β_y are the rotations of the middle plane around the

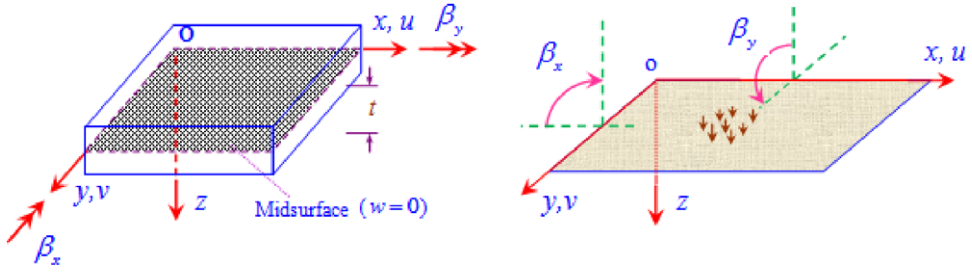

Figure 2. The Reissner–Mindlin plate and positive directions of the displacements u, v, w and two rotations β_x, β_y.

y- and x-axes, respectively, with the positive directions defined in figure 2.

The linear strain can be given by

$$\begin{Bmatrix} \varepsilon_x \\ \varepsilon_y \\ \gamma_{xy} \end{Bmatrix} = \begin{Bmatrix} u_{0,x} \\ v_{0,y} \\ u_{0,x} + v_{0,y} \end{Bmatrix} + z \begin{Bmatrix} \beta_{x,x} \\ \beta_{y,y} \\ \beta_{x,y} + \beta_{y,x} \end{Bmatrix} = \boldsymbol{\varepsilon}_0 + z\boldsymbol{\kappa} \tag{6}$$

$$\begin{Bmatrix} \gamma_{xz} \\ \gamma_{yz} \end{Bmatrix} = \begin{Bmatrix} w_{,x} + \beta_x \\ w_{,y} + \beta_y \end{Bmatrix} = \boldsymbol{\gamma}. \tag{7}$$

In the laminated composite plate, the constitutive equation of the kth orthotropic layer in local coordinates is derived from Hook's law for plane stress as

$$\begin{Bmatrix} \sigma_{xx} \\ \sigma_{yy} \\ \tau_{xy} \\ \tau_{xz} \\ \tau_{yz} \end{Bmatrix}^{(k)} = \begin{bmatrix} Q_{11} & Q_{12} & Q_{16} & 0 & 0 \\ Q_{21} & Q_{22} & Q_{26} & 0 & 0 \\ Q_{61} & Q_{62} & Q_{66} & 0 & 0 \\ 0 & 0 & 0 & Q_{55} & Q_{54} \\ 0 & 0 & 0 & Q_{45} & Q_{44} \end{bmatrix}^{(k)} \begin{Bmatrix} \varepsilon_{xx} \\ \varepsilon_{yy} \\ \gamma_{xy} \\ \gamma_{xz} \\ \gamma_{yz} \end{Bmatrix}^{(k)} \tag{8}$$

where the material constants are given by

$$\begin{aligned} Q_{11} &= \frac{E_1}{1 - \nu_{12}\nu_{21}}, & Q_{12} &= \frac{\nu_{12}E_2}{1 - \nu_{12}\nu_{21}}, \\ Q_{22} &= \frac{E_2}{1 - \nu_{12}\nu_{21}}, & Q_{66} &= G_{12}, \\ Q_{55} &= G_{13}, & Q_{44} &= G_{23} \end{aligned} \tag{9}$$

in which E_1, E_2 are the Young's moduli in the 1 and 2 directions, respectively, G_{12}, G_{23}, G_{13} are the shear moduli in the 1–2, 2–3 and 3–1 planes, respectively, and ν_{ij} are the Poisson's ratios.

The laminate is usually made of several orthotropic layers in which the stress–strain relation for the kth orthotropic lamina (with arbitrary fiber orientation compared to the reference axes) is computed by

$$\begin{Bmatrix} \sigma_{xx} \\ \sigma_{yy} \\ \tau_{xy} \\ \tau_{xz} \\ \tau_{yz} \end{Bmatrix}^{(k)} = \begin{bmatrix} \bar{Q}_{11} & \bar{Q}_{12} & \bar{Q}_{16} & 0 & 0 \\ \bar{Q}_{21} & \bar{Q}_{22} & \bar{Q}_{26} & 0 & 0 \\ \bar{Q}_{61} & \bar{Q}_{62} & \bar{Q}_{66} & 0 & 0 \\ 0 & 0 & 0 & \bar{Q}_{55} & \bar{Q}_{54} \\ 0 & 0 & 0 & \bar{Q}_{45} & \bar{Q}_{44} \end{bmatrix}^{(k)} \begin{Bmatrix} \varepsilon_{xx} \\ \varepsilon_{yy} \\ \gamma_{xy} \\ \gamma_{xz} \\ \gamma_{yz} \end{Bmatrix}^{(k)} \tag{10}$$

where the $\bar{Q}_{ij}$ are transformed material constants of the kth lamina [76].

From Hook's law and the linear strains given by equations (6) and (7), the stress is computed by

$$\boldsymbol{\sigma} = \begin{bmatrix} \boldsymbol{\sigma}_\mathrm{p} \\ \boldsymbol{\tau} \end{bmatrix} = \underbrace{\begin{bmatrix} \bar{\mathbf{D}} & \mathbf{0} \\ \mathbf{0} & \bar{\mathbf{D}}_\mathrm{s} \end{bmatrix}}_{\mathbf{c}} \underbrace{\begin{bmatrix} \boldsymbol{\varepsilon}_\mathrm{p} \\ \boldsymbol{\gamma} \end{bmatrix}}_{\boldsymbol{\varepsilon}} = \mathbf{c}\boldsymbol{\varepsilon} \tag{11}$$

where $\boldsymbol{\varepsilon}_\mathrm{p} = \begin{bmatrix} \boldsymbol{\varepsilon}_0 & \boldsymbol{\kappa} \end{bmatrix}^\mathrm{T}$; $\boldsymbol{\sigma}_\mathrm{p}$ and $\boldsymbol{\tau}$ are the in-plane stress component and shear stress; $\bar{\mathbf{D}}$ and $\bar{\mathbf{D}}_\mathrm{s}$ are material constant matrices given in the form of

$$\bar{\mathbf{D}} = \begin{bmatrix} \mathbf{D}_\mathrm{m} & \mathbf{B} \\ \mathbf{B} & \mathbf{D}_\mathrm{b} \end{bmatrix} \qquad \bar{\mathbf{D}}_\mathrm{s} = k \int_{-t/2}^{t/2} \bar{Q}_{ij}\,\mathrm{d}z$$
$$i, j = 4, 5\ (k = 5/6) \tag{12}$$

in which

$$\begin{aligned} \mathbf{D}_{mij} &= \int_{-t/2}^{t/2} \bar{Q}_{ij}\,\mathrm{d}z; & \mathbf{B}_{ij} &= \int_{-t/2}^{t/2} z\bar{Q}_{ij}\,\mathrm{d}z; \\ \mathbf{D}_{bij} &= \int_{-t/2}^{t/2} z^2\bar{Q}_{ij}\,\mathrm{d}z & & (i, j = 1, 2, 6). \end{aligned} \tag{13}$$

Note that the parameter $k = 5/6$ in equation (12) aims to ensure a more accurate approximation of the shear stress [76].

2.3.2. FEM formulation for a laminated composite plate. Now, by discretizing the bounded domain Ω of the composite plate into N_e finite elements such that $\Omega = \bigcup_{e=1}^{N_\mathrm{e}} \Omega_\mathrm{e}$ and $\Omega_i \cap \Omega_j = \varnothing$, $i \neq j$, the finite element solution $\mathbf{u}^h = \begin{bmatrix} u & v & w & \beta_x & \beta_y \end{bmatrix}^\mathrm{T}$ of the laminated composite plate is expressed as

$$\mathbf{u}^h = \sum_{i=1}^{N_\mathrm{n}} \begin{bmatrix} N_i & 0 & 0 & 0 & 0 \\ 0 & N_i & 0 & 0 & 0 \\ 0 & 0 & N_i & 0 & 0 \\ 0 & 0 & 0 & N_i & 0 \\ 0 & 0 & 0 & 0 & N_i \end{bmatrix} \mathbf{d}_i = \mathbf{N}\mathbf{d} \tag{14}$$

where N_n is the total number of nodes of the problem domain discretized, N_i is the shape function at the ith node and $\mathbf{d}_i = [u_i\ v_i\ w_i\ \beta_{xi}\ \beta_{yi}]^\mathrm{T}$ is the displacement vector of the nodal degrees of freedom of $\mathbf{u}^h$ associated to the ith node.

The membrane, bending and shear strains can be then expressed in matrix form as

$$\boldsymbol{\varepsilon}_0 = \sum_i \mathbf{B}_i^{\mathrm{m}} \mathbf{d}_i; \qquad \boldsymbol{\kappa} = \sum_i \mathbf{B}_i^{\mathrm{b}} \mathbf{d}_i; \qquad \boldsymbol{\gamma} = \sum_i \mathbf{B}_i^{\mathrm{s}} \mathbf{d}_i \tag{15}$$

where

$$\mathbf{B}_i^{\mathrm{m}} = \begin{bmatrix} N_{i,x} & 0 & 0\,0\,0 \\ 0 & N_{i,y} & 0\,0\,0 \\ N_{i,y} & N_{i,x} & 0\,0\,0 \end{bmatrix};$$
$$\mathbf{B}_i^{\mathrm{b}} = \begin{bmatrix} 0\,0\,0 & N_{i,x} & 0 \\ 0\,0\,0 & 0 & N_{i,y} \\ 0\,0\,0 & N_{i,y} & N_{i,x} \end{bmatrix}; \tag{16}$$
$$\mathbf{B}_i^{\mathrm{s}} = \begin{bmatrix} 0\,0 & N_{i,x} & N_i & 0 \\ 0\,0 & N_{i,y} & 0 & N_i \end{bmatrix}$$

in which $N_{i,x}$ and $N_{i,y}$ are the derivatives of the shape functions in the x- and y-directions, respectively.

2.3.3. Formulation of the CS-FEM-DSG3 for a laminated composite plate.

Q.6 *2.3.3.1. Brief on the DSG3 formulation.* In the DSG3 [75], the problem domain is discretized into a mesh of three-node triangular elements, and the formulation is based on the concept of the 'shear gap' of the displacement along the edges of the elements. In the original DSG3, the first-order shear deformation plate theory (FSDT) is used for Mindlin plate behavior and each node only has three degrees of freedom $\mathbf{d}_i = [w_i\ \beta_{xi}\ \beta_{yi}]^{\mathrm{T}}$. The DSG3 element is shear-locking-free and has several superior properties, as presented in [75].

In this paper, the DSG3 is extended to the laminated composite plate and each node will have five degrees of freedom. The approximation $\mathbf{u}^h = [u\ v\ w\ \beta_x\ \beta_y]^{\mathrm{T}}$ for a three-node triangular element Ω_{e} shown in figure 3 for the laminated composite plate can be written, at the element level, as

$$\mathbf{u}^h = \sum_{I=1}^{N_{\mathrm{n}}} \begin{bmatrix} N_I & 0 & 0 & 0 & 0 \\ 0 & N_I & 0 & 0 & 0 \\ 0 & 0 & N_I & 0 & 0 \\ 0 & 0 & 0 & N_I & 0 \\ 0 & 0 & 0 & 0 & N_I \end{bmatrix} \mathbf{d}_I = \mathbf{N}\mathbf{d} \tag{17}$$

where $\mathbf{d}_I = [u_I\ v_I\ w_I\ \beta_{xI}\ \beta_{yI}]^{\mathrm{T}}$ are the nodal degrees of freedom of $\mathbf{u}_{\mathrm{e}}^h$ associated to node I and the N_I are linear shape functions in natural coordinates defined by

$$N_1 = 1 - \xi - \eta, \qquad N_2 = \xi, \qquad N_3 = \eta. \tag{18}$$

The membrane strain and the curvatures of deflection in the element are obtained by

$$\boldsymbol{\varepsilon}_0 = \mathbf{B}^{\mathrm{m}}\mathbf{d}_{\mathrm{e}}; \qquad \boldsymbol{\kappa} = \mathbf{B}^{\mathrm{b}}\mathbf{d}_{\mathrm{e}}; \qquad \boldsymbol{\gamma} = \mathbf{B}^{\mathrm{s}}\mathbf{d}_{\mathrm{e}} \tag{19}$$

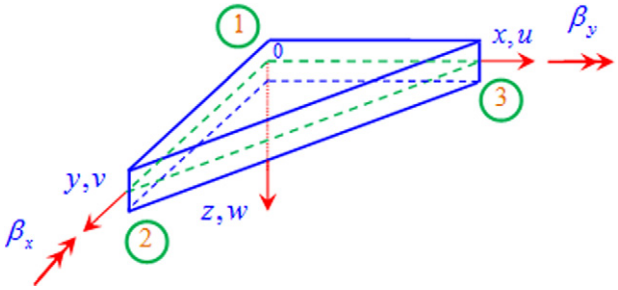

Figure 3. A three-node triangular element.

where $\mathbf{d}_{\mathrm{e}} = [\mathbf{d}_{\mathrm{e}1}\ \mathbf{d}_{\mathrm{e}2}\ \mathbf{d}_{\mathrm{e}3}]^{\mathrm{T}}$ is the nodal displacement vector of the element; $\mathbf{B}_i^{\mathrm{m}}$, $\mathbf{B}_i^{\mathrm{b}}$ and $\mathbf{B}_i^{\mathrm{s}}$ $(i = 1\text{–}3)$ contain the derivatives of the shape functions that are constants

$$\mathbf{B}^{\mathrm{m}} = \frac{1}{2A_{\mathrm{e}}} \times \begin{bmatrix} b-c & 0 & 0\,0\,0 & c & 0\,0\,0 & -b & 0 & 0\,0\,0 \\ 0 & d-a & 0\,0\,0 & -d & 0\,0\,0 & 0 & a & 0\,0\,0 \\ d-a & b-c & 0\,0\,0 & -d & c & 0\,0\,0 & a & -b & 0\,0\,0 \end{bmatrix}$$
$$= \frac{1}{2A_{\mathrm{e}}} \begin{bmatrix} \mathbf{B}_1^{\mathrm{m}} & \mathbf{B}_2^{\mathrm{m}} & \mathbf{B}_3^{\mathrm{m}} \end{bmatrix} \tag{20}$$

$$\mathbf{B}^{\mathrm{b}} = \frac{1}{2A_{\mathrm{e}}} \times \begin{bmatrix} 0\,0\,0 & b-c & 0 & 0\,0\,0 & c & -d & 0\,0\,0 & -b & 0 \\ 0\,0\,0 & 0 & d-a & 0\,0\,0 & 0 & 0 & 0\,0\,0 & 0 & a \\ 0\,0\,0 & d-a & b-c & 0\,0\,0 & -d & c & 0\,0\,0 & a & -b \end{bmatrix}$$
$$= \frac{1}{2A_{\mathrm{e}}} \begin{bmatrix} \mathbf{B}_1^{\mathrm{b}} & \mathbf{B}_2^{\mathrm{b}} & \mathbf{B}_3^{\mathrm{b}} \end{bmatrix} \tag{21}$$

$$\mathbf{B}^{\mathrm{s}} = \frac{1}{2A_{\mathrm{e}}} \begin{bmatrix} 0\,0 & b-c & A_{\mathrm{e}} & 0 & 0\,0 & c & \frac{ac}{2} & \frac{bc}{2} & 0\,0 & -b & \frac{-bd}{2} & \frac{-bc}{2} \\ 0\,0 & d-a & 0 & A_{\mathrm{e}} & 0\,0 & -d & \frac{-ad}{2} & \frac{-bd}{2} & 0\,0 & a & \frac{ad}{2} & \frac{ac}{2} \end{bmatrix}$$
$$= \frac{1}{2A_{\mathrm{e}}} \begin{bmatrix} \mathbf{B}_1^{\mathrm{s}} & \mathbf{B}_2^{\mathrm{s}} & \mathbf{B}_3^{\mathrm{s}} \end{bmatrix} \tag{22}$$

where a, b, c and d are the geometric distances as shown in figure 4; A_{e} is the area of the triangular element.

From equations (20) to (22), it is clearly seen that the element stiffness matrix in the DSG3 depends on the sequence of node numbers of elements, and hence the solution of the DSG3 is influenced when the sequence of node numbers of elements is changed, especially for coarse and distorted meshes. In addition, as shown in previous numerical

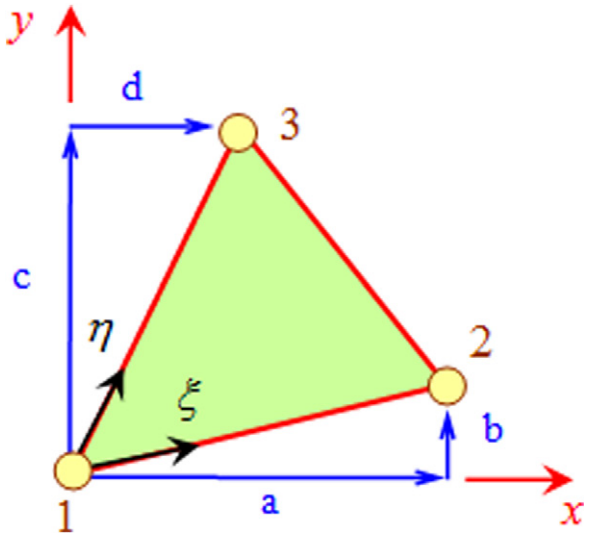

Figure 4. A three-node triangular element and local coordinates in the DSG3.

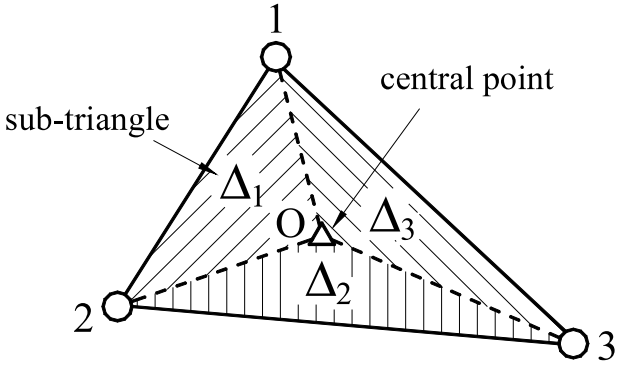

Figure 5. Three sub-triangles (Δ_1, Δ_2 and Δ_3) created from the triangle 1–2–3 in the CS-FEM-DSG3 by connecting the central point O with three field nodes 1–3.

analyses [74], the DSG3 still possesses the over-stiff property which can lead to poor accuracy of solutions. The gradient smoothing technique in the CS-FEM [32, 33] is hence proposed to combine with the DSG3 to help to overcome these two drawbacks.

2.3.3.2. Formulation of the CS-FEM-DSG3. In the original CS-FEM-DSG3 [74], the domain discretization is the same as that of the DSG3 [75] using N_n nodes and N_e triangular elements. However, in the formulation of the CS-FEM-DSG3, each triangular element Ω_e is further divided into three sub-triangles Δ_1, Δ_2 and Δ_3 by connecting the central point O of the element to three field nodes as shown in figure 5.

In the CS-FEM-DSG3, we assume that the displacement vector $\mathbf{d}_O^e$ at the central point O is the simple average of three displacement vectors $\mathbf{d}_1^e$, $\mathbf{d}_2^e$ and $\mathbf{d}_3^e$ of three field nodes

$$\mathbf{d}_O^e = \tfrac{1}{3}\left(\mathbf{d}_1^e + \mathbf{d}_2^e + \mathbf{d}_3^e\right). \tag{23}$$

On the first sub-triangle Δ_1 (triangle O–1–2), the linear approximation $\mathbf{u}^{e\Delta_1} = [u^{e\Delta_1} \;\; v^{e\Delta_1} \;\; w^{e\Delta_1} \;\; \beta_x^{e\Delta_1} \;\; \beta_y^{e\Delta_1}]^T$ is constructed by

$$\mathbf{u}^{e\Delta_1} = N_1^{e\Delta_1}\mathbf{d}_O^e + N_2^{e\Delta_1}\mathbf{d}_1^e + N_3^{e\Delta_1}\mathbf{d}_2^e = \mathbf{N}^{e\Delta_1}\mathbf{d}^{e\Delta_1} \tag{24}$$

where $\mathbf{d}^{e\Delta_1} = [\mathbf{d}_O^e \;\; \mathbf{d}_1^e \;\; \mathbf{d}_2^e]^T$ is the vector of nodal degrees of freedom of the sub-triangle Δ_1 and $\mathbf{N}^{e\Delta_1} = [N_1^{e\Delta_1} \;\; N_2^{e\Delta_1} \;\; N_3^{e\Delta_1}]$ contains the linear shape functions created by the sub-triangle Δ_1.

Using the DSG3 formulation [74, 75] for the sub-triangle Δ_1, the membrane, bending and shear strains $\boldsymbol{\varepsilon}_0^{e\Delta_1}$, $\boldsymbol{\kappa}^{e\Delta_1}$ and $\boldsymbol{\gamma}^{e\Delta_1}$ in the sub-triangle Δ_1 are then obtained, respectively, by

$$\boldsymbol{\varepsilon}_0^{e\Delta_1} = \underbrace{\left[\mathbf{b}_1^{m\Delta_1} \;\; \mathbf{b}_2^{m\Delta_1} \;\; \mathbf{b}_3^{m\Delta_1}\right]}_{\mathbf{b}^{m\Delta_1}} \begin{bmatrix}\mathbf{d}_O^e\\ \mathbf{d}_1^e\\ \mathbf{d}_2^e\end{bmatrix} = \mathbf{b}^{m\Delta_1}\mathbf{d}^{e\Delta_1} \tag{25}$$

$$\boldsymbol{\kappa}^{e\Delta_1} = \underbrace{\left[\mathbf{b}_1^{b\Delta_1} \;\; \mathbf{b}_2^{b\Delta_1} \;\; \mathbf{b}_3^{b\Delta_1}\right]}_{\mathbf{b}^{b\Delta_1}} \begin{bmatrix}\mathbf{d}_O^e\\ \mathbf{d}_1^e\\ \mathbf{d}_2^e\end{bmatrix} = \mathbf{b}^{b\Delta_1}\mathbf{d}^{e\Delta_1} \tag{26}$$

$$\boldsymbol{\gamma}^{e\Delta_1} = \underbrace{\left[\mathbf{b}_1^{s\Delta_1} \;\; \mathbf{b}_2^{s\Delta_1} \;\; \mathbf{b}_3^{s\Delta_1}\right]}_{\mathbf{b}^{s\Delta_1}} \begin{bmatrix}\mathbf{d}_O^e\\ \mathbf{d}_1^e\\ \mathbf{d}_2^e\end{bmatrix} = \mathbf{b}^{s\Delta_1}\mathbf{d}^{e\Delta_1} \tag{27}$$

where $\mathbf{b}^{m\Delta_1}$, $\mathbf{b}^{b\Delta_1}$ and $\mathbf{b}^{s\Delta_1}$ are, respectively, computed similarly to the matrices $\mathbf{B}^m$, $\mathbf{B}^b$ and $\mathbf{B}^s$ in equations (20)–(22) but with the following two changes: (1) the coordinates of the three nodes $i = 1$–3 are replaced by $\mathbf{x}_O$, $\mathbf{x}_1$ and $\mathbf{x}_2$, respectively; and (2) the area A_e is replaced by the area A_{Δ_1} of sub-triangle Δ_1.

Substituting $\mathbf{d}_O^e$ in equation (23) into (25)–(27), and then rearranging, we obtain

$$\boldsymbol{\varepsilon}_0^{e\Delta_1} = \underbrace{\left[\tfrac{1}{3}\mathbf{b}_1^{m\Delta_1} + \mathbf{b}_2^{m\Delta_1} \;\; \tfrac{1}{3}\mathbf{b}_1^{m\Delta_1} + \mathbf{b}_3^{m\Delta_1} \;\; \tfrac{1}{3}\mathbf{b}_1^{m\Delta_1}\right]}_{\mathbf{B}^{m\Delta_1}} \begin{bmatrix}\mathbf{d}_1^e\\ \mathbf{d}_2^e\\ \mathbf{d}_3^e\end{bmatrix} = \mathbf{B}^{m\Delta_1}\mathbf{d}^e \tag{28}$$

$$\boldsymbol{\kappa}^{e\Delta_1} = \underbrace{\left[\tfrac{1}{3}\mathbf{b}_1^{b\Delta_1} + \mathbf{b}_2^{b\Delta_1} \;\; \tfrac{1}{3}\mathbf{b}_1^{b\Delta_1} + \mathbf{b}_3^{b\Delta_1} \;\; \tfrac{1}{3}\mathbf{b}_1^{b\Delta_1}\right]}_{\mathbf{B}^{b\Delta_1}} \begin{bmatrix}\mathbf{d}_1^e\\ \mathbf{d}_2^e\\ \mathbf{d}_3^e\end{bmatrix} = \mathbf{B}^{b\Delta_1}\mathbf{d}^e \tag{29}$$

$$\boldsymbol{\gamma}^{e\Delta_1} = \underbrace{\left[\tfrac{1}{3}\mathbf{b}_1^{s\Delta_1} + \mathbf{b}_2^{s\Delta_1} \;\; \tfrac{1}{3}\mathbf{b}_1^{s\Delta_1} + \mathbf{b}_3^{s\Delta_1} \;\; \tfrac{1}{3}\mathbf{b}_1^{s\Delta_1}\right]}_{\mathbf{B}^{s\Delta_1}} \begin{bmatrix}\mathbf{d}_1^e\\ \mathbf{d}_2^e\\ \mathbf{d}_3^e\end{bmatrix} = \mathbf{B}^{s\Delta_1}\mathbf{d}^e. \tag{30}$$

Similarly, by using cyclic permutation, we easily obtain the bending and shear strains $\boldsymbol{\varepsilon}_0^{e\Delta_j}$, $\boldsymbol{\kappa}^{e\Delta_j}$, $\boldsymbol{\gamma}^{e\Delta_j}$ and matrices $\mathbf{B}^{m\Delta_j}$, $\mathbf{B}^{b\Delta_j}$, $\mathbf{B}^{s\Delta_j}$, $j = 2, 3$, for the second sub-triangle Δ_2 (triangle O–2–3) and third sub-triangle Δ_3 (triangle O–3–1), respectively.

Now, applying the cell-based strain smoothing operation in the CS-FEM [32, 33], the constant membrane, bending and

shear strains $\boldsymbol{\varepsilon}_0^{e\Delta_j}$, $\boldsymbol{\kappa}^{e\Delta_j}, \boldsymbol{\gamma}^{e\Delta_j}, j = 1, 2, 3$, are, respectively, used to create element smoothed strains $\tilde{\boldsymbol{\varepsilon}}_0^e$, $\tilde{\boldsymbol{\kappa}}^e$ and $\tilde{\boldsymbol{\gamma}}^e$ on the triangular element Ω_e, such as

$$\tilde{\boldsymbol{\varepsilon}}_0^e = \int_{\Omega_e} \boldsymbol{\varepsilon}_0^h \, \Phi_e(\mathbf{x}) \, d\Omega = \sum_{j=1}^{3} \boldsymbol{\varepsilon}_0^{\Delta_j} \int_{\Delta_j} \Phi_e(\mathbf{x}) \, d\Omega \tag{31}$$

$$\tilde{\boldsymbol{\kappa}}^e = \int_{\Omega_e} \boldsymbol{\kappa}^h \, \Phi_e(\mathbf{x}) \, d\Omega = \sum_{j=1}^{3} \boldsymbol{\kappa}^{e\Delta_j} \int_{\Delta_j} \Phi_e(\mathbf{x}) \, d\Omega \tag{32}$$

$$\tilde{\boldsymbol{\gamma}}^e = \int_{\Omega_e} \boldsymbol{\gamma}^h \, \Phi_e(\mathbf{x}) \, d\Omega = \sum_{j=1}^{3} \boldsymbol{\gamma}^{e\Delta_j} \int_{\Delta_j} \Phi_e(\mathbf{x}) \, d\Omega \tag{33}$$

where $\Phi_e(\mathbf{x})$ is a given smoothing function that satisfies the unity property $\int_{\Omega_e} \Phi_e(\mathbf{x}) \, d\Omega = 1$. Using the following Heaviside constant smoothing function:

$$\Phi_e(\mathbf{x}) = \begin{cases} 1/A_e & \mathbf{x} \in \Omega_e \\ 0 & \mathbf{x} \notin \Omega_e \end{cases} \tag{34}$$

where A_e is the area of the triangular element, the element smoothed strains $\tilde{\boldsymbol{\varepsilon}}_0^e$, $\tilde{\boldsymbol{\kappa}}^e$ and $\tilde{\boldsymbol{\gamma}}^e$ in equations (31)–(33) become

$$\begin{gathered} \tilde{\boldsymbol{\varepsilon}}_0^e = \frac{1}{A_e} \sum_{j=1}^{3} A_{\Delta_j} \boldsymbol{\varepsilon}_0^{e\Delta_j}; \\ \tilde{\boldsymbol{\kappa}}^e = \frac{1}{A_e} \sum_{j=1}^{3} A_{\Delta_j} \boldsymbol{\kappa}^{e\Delta_j}; \qquad \tilde{\boldsymbol{\gamma}}^e = \frac{1}{A_e} \sum_{j=1}^{3} A_{\Delta_j} \boldsymbol{\gamma}^{e\Delta_j}. \end{gathered} \tag{35}$$

Substituting $\boldsymbol{\varepsilon}_0^{e\Delta_j}$, $\boldsymbol{\kappa}^{e\Delta_j}$ and $\boldsymbol{\gamma}^{e\Delta_j}, j = 1$–$3$, into equation (35), the element smoothed strains $\tilde{\boldsymbol{\varepsilon}}_0^e$, $\tilde{\boldsymbol{\kappa}}^e$ and $\tilde{\boldsymbol{\gamma}}^e$ are now expressed by

$$\tilde{\boldsymbol{\varepsilon}}_0^e = \tilde{\mathbf{B}}^m \mathbf{d}^e; \qquad \tilde{\boldsymbol{\kappa}}^e = \tilde{\mathbf{B}}^b \mathbf{d}^e; \qquad \tilde{\boldsymbol{\gamma}}^e = \tilde{\mathbf{B}}^s \mathbf{d}^e \tag{36}$$

where $\tilde{\mathbf{B}}^m$, $\tilde{\mathbf{B}}^b$ and $\tilde{\mathbf{B}}^s$ are the smoothed strain gradient matrices, respectively, given by

$$\begin{gathered} \tilde{\mathbf{B}}^m = \frac{1}{A_e} \sum_{j=1}^{3} A_{\Delta_j} \mathbf{B}^{m\Delta_j}; \\ \tilde{\mathbf{B}}^b = \frac{1}{A_e} \sum_{j=1}^{3} A_{\Delta_j} \mathbf{B}^{b\Delta_j}; \qquad \tilde{\mathbf{B}}^s = \frac{1}{A_e} \sum_{j=1}^{3} A_{\Delta_j} \mathbf{B}^{s\Delta_j}. \end{gathered} \tag{37}$$

Therefore, the stress of the CS-FEM-DSG3 is expressed as

$$\boldsymbol{\sigma} = \underbrace{\begin{bmatrix} \bar{\mathbf{D}} & \mathbf{0} \\ \mathbf{0} & \bar{\mathbf{D}}_s \end{bmatrix}}_{\mathbf{c}} \underbrace{\begin{bmatrix} \tilde{\boldsymbol{\varepsilon}}_p \\ \tilde{\boldsymbol{\gamma}} \end{bmatrix}}_{\tilde{\boldsymbol{\varepsilon}}} = \mathbf{c}\tilde{\boldsymbol{\varepsilon}} \tag{38}$$

in which

$$\tilde{\boldsymbol{\varepsilon}}_p = \begin{bmatrix} \tilde{\boldsymbol{\varepsilon}}_0 & \tilde{\boldsymbol{\kappa}} \end{bmatrix}^T. \tag{39}$$

From equations (35)–(37), it is clearly seen that the element strain matrix in the CS-FEM-DSG3 does not depend on the sequence of node numbers, and hence the solution of the CS-FEM-DSG3 is unchanged when the sequence of node numbers changes. In addition, due to using the gradient smoothing technique in the CS-FEM [32, 33] which helps to soften the over-stiff behavior in the DSG3, the CS-FEM-DSG3 will significantly improve the accuracy of the numerical results by the DSG3.

2.4. Approximations of the electric potential

In this study, approximations of the electric potential field of each piezoelectric layer are made by discretization of each piezoelectric layer into finite sublayers along the thickness direction. In each sublayer, a linear electric potential function is approximated through the thickness by [12]

$$\phi^i(z) = \mathbf{N}_\phi^i \boldsymbol{\phi}^i \tag{40}$$

where $\mathbf{N}_\phi^i$ and $\boldsymbol{\phi}^i$ are, respectively, the shape function of the electric potential function and the electric potentials at the top and bottom surfaces of the sublayer, and are defined as

$$\begin{aligned} \mathbf{N}_\phi^i &= \frac{1}{h_i} \begin{bmatrix} z_i - z & z - z_{i-1} \end{bmatrix} \qquad (h_i = z_{i-1} - z_i) \\ \boldsymbol{\phi}^i &= \begin{bmatrix} \phi^{i-1} & \phi^i \end{bmatrix} \qquad (i = 1, 2, \ldots, n_{sub}) \end{aligned} \tag{41}$$

in which n_{sub} is the number of piezoelectric layers.

For each piezoelectric sublayer element, it is assumed that the electric potentials at the same height along the thickness have the same behavior [15, 25]. Hence, for each sublayer element, the electric field $\mathbf{E}$ in equation (2) can be rewritten as

$$\mathbf{E} = \underbrace{-\nabla \mathbf{N}_\phi^i}_{\mathbf{B}_\phi} \boldsymbol{\phi}^i = -\mathbf{B}_\phi \boldsymbol{\phi}^i. \tag{42}$$

Note that the piezoelectric constant matrix $\mathbf{e}$ and the dielectric constant matrix $\mathbf{g}$ of the kth orthotropic layer in local coordinates are derived by [12]

$$\begin{aligned} \mathbf{e}^{(k)} &= \begin{bmatrix} 0 & 0 & 0 & 0 & d_{15} & 0 \\ 0 & 0 & 0 & d_{15} & 0 & 0 \\ d_{31} & d_{31} & d_{33} & 0 & 0 & 0 \end{bmatrix}^{(k)}; \\ \mathbf{g}^{(k)} &= \begin{bmatrix} p_{11} & 0 & 0 \\ 0 & p_{22} & 0 \\ 0 & 0 & p_{33} \end{bmatrix}^{(k)}. \end{aligned} \tag{43}$$

In addition, the laminate is usually made of several orthotropic layers in which the piezoelectric constant matrix for the kth orthotropic lamina is given by

$$\begin{aligned} \mathbf{e}^{(k)} &= \begin{bmatrix} 0 & 0 & 0 & 0 & \bar{d}_{15} & 0 \\ 0 & 0 & 0 & \bar{d}_{15} & 0 & 0 \\ \bar{d}_{31} & \bar{d}_{31} & \bar{d}_{33} & 0 & 0 & 0 \end{bmatrix}^{(k)}; \\ \mathbf{g}^{(k)} &= \begin{bmatrix} \bar{p}_{11} & 0 & 0 \\ 0 & \bar{p}_{22} & 0 \\ 0 & 0 & \bar{p}_{33} \end{bmatrix}^{(k)} \end{aligned} \tag{44}$$

where $\bar{d}_{ij}$ and $\bar{p}_{ii}$ are transformed material constants of the kth lamina and are calculated similarly to $\bar{Q}_{ij}$ in equation (10).

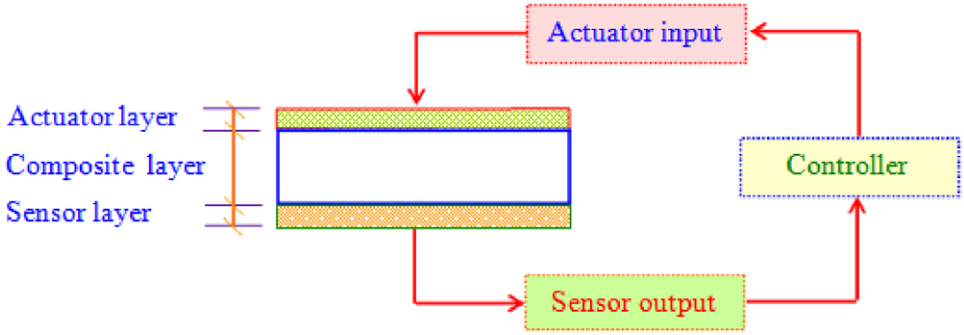

Figure 6. A schematic diagram of a laminate plate with integrated piezoelectric sensors and actuators.

2.5. Elementary governing equation of motion

The elementary governing equation of motion can be derived by substituting equations (11), (36), (40) and (42) into equation (4), and assembling the electric potentials along the thickness. The final form of this equation is then written in the form

$$\begin{bmatrix} \mathbf{M}_{uu} & 0 \\ 0 & 0 \end{bmatrix} \begin{bmatrix} \ddot{\mathbf{d}} \\ \ddot{\boldsymbol{\phi}} \end{bmatrix} + \begin{bmatrix} \mathbf{K}_{uu} & \mathbf{K}_{u\phi} \\ \mathbf{K}_{\phi u} & \mathbf{K}_{\phi\phi} \end{bmatrix} \begin{bmatrix} \mathbf{d} \\ \boldsymbol{\phi} \end{bmatrix} = \begin{bmatrix} \mathbf{F} \\ \mathbf{Q} \end{bmatrix} \tag{45}$$

where

$$\begin{aligned} \mathbf{K}_{uu} &= \int_{\Omega} \tilde{\mathbf{B}}_u^{\mathrm{T}} \mathbf{c} \tilde{\mathbf{B}}_u \, \mathrm{d}\Omega = \tilde{\mathbf{B}}_u^{\mathrm{T}} \mathbf{c} \tilde{\mathbf{B}}_u A; \\ \mathbf{K}_{u\phi} &= \int_{\Omega} \tilde{\mathbf{B}}_u^{\mathrm{T}} \mathbf{e}^{\mathrm{T}} \mathbf{B}_\phi \, \mathrm{d}\Omega = \tilde{\mathbf{B}}_u^{\mathrm{T}} \mathbf{e}^{\mathrm{T}} \mathbf{B}_\phi A; \\ \mathbf{K}_{\phi\phi} &= -\int_{\Omega} \mathbf{B}_\phi^{\mathrm{T}} \mathbf{p} \mathbf{B}_\phi \, \mathrm{d}\Omega = \mathbf{B}_\phi^{\mathrm{T}} \mathbf{p} \mathbf{B}_\phi A; \\ \mathbf{M}_{uu} &= \int_{\Omega} \mathbf{N}^{\mathrm{T}} \mathbf{m} \mathbf{N} \, \mathrm{d}\Omega \end{aligned} \tag{46}$$

in which $\tilde{\mathbf{B}}_u = [\tilde{\mathbf{B}}^{\mathrm{m}} \ \tilde{\mathbf{B}}^{\mathrm{b}} \ \tilde{\mathbf{B}}^{\mathrm{s}}]^{\mathrm{T}}$ and $\mathbf{m}$ is defined by [60]

$$\mathbf{m} = \rho t \begin{bmatrix} 1 & 0 & 0 & 0 & 0 \\ 0 & 1 & 0 & 0 & 0 \\ 0 & 0 & 1 & 0 & 0 \\ 0 & 0 & 0 & \dfrac{t^2}{12} & 0 \\ 0 & 0 & 0 & 0 & \dfrac{t^2}{12} \end{bmatrix}. \tag{47}$$

Substituting the second equation of (45) into the first equation of (45), we obtain a shortened form as

$$\mathbf{M}\ddot{\mathbf{d}} + (\mathbf{K}_{uu} + \mathbf{K}_{u\phi}\mathbf{K}_{\phi\phi}^{-1}\mathbf{K}_{\phi u})\mathbf{d} = \mathbf{F} + \mathbf{K}_{u\phi}\mathbf{K}_{\phi\phi}^{-1}\mathbf{Q}. \tag{48}$$

3. Active control analysis

We now consider a piezoelectric laminated composite plate with n layers as shown in figure 6. The top layer is a piezoelectric actuator denoted with subscript a and the bottom layer is a piezoelectric sensor labeled with subscript s. In this work, the displacement feedback control [15], which helps the piezoelectric actuator to generate the charge, is combined with velocity feedback control [21–25, 6, 26, 27], which can give a velocity component by using an appropriate electronic circuit. In addition, a consistent method [4, 26] which can predict the dynamic responses of smart piezoelectric composite plates is adopted. The constant gains G_{d} and G_{v} of the displacement feedback control and velocity feedback control [26] are hence used to couple the input actuator voltage vector $\boldsymbol{\phi}_{\mathrm{a}}$ and the output sensor voltage $\boldsymbol{\phi}_{\mathrm{s}}$ as

$$\boldsymbol{\phi}_{\mathrm{a}} = G_{\mathrm{d}}\boldsymbol{\phi}_{\mathrm{s}} + G_{\mathrm{v}}\dot{\boldsymbol{\phi}}_{\mathrm{s}}. \tag{49}$$

Without the external charge $\mathbf{Q}$, the generated potential on the sensor layer can be derived from the second equation of (45) as

$$\boldsymbol{\phi}_{\mathrm{s}} = \left[\mathbf{K}_{\phi\phi}^{-1}\right]_{\mathrm{s}} \left[\mathbf{K}_{\phi u}\right]_{\mathrm{s}} \mathbf{d}_{\mathrm{s}} \tag{50}$$

which implies that when the plate is deformed by an external force, electric charges are generated in the sensor layer and are amplified through closed loop control to convert into the signal. The converted signal is then sent to the distributed actuator and an input voltage for the actuators is generated through the converse piezoelectric effect. Finally, a resultant force is formed to actively control the static response of the laminated composite plate.

The magnitude of the voltage is defined by substituting equations (49) and (50) into the second equation of (45) as

$$\begin{aligned} \mathbf{Q}_{\mathrm{a}} = {} & [\mathbf{K}_{uu}]_{\mathrm{a}} \mathbf{d}_{\mathrm{a}} - G_{\mathrm{d}} \left[\mathbf{K}_{\phi\phi}\right]_{\mathrm{a}} \left[\mathbf{K}_{\phi\phi}^{-1}\right]_{\mathrm{s}} \left[\mathbf{K}_{\phi u}\right]_{\mathrm{s}} \mathbf{d}_{\mathrm{s}} \\ & - G_{\mathrm{v}} \left[\mathbf{K}_{\phi\phi}\right]_{\mathrm{a}} \left[\mathbf{K}_{\phi\phi}^{-1}\right]_{\mathrm{s}} \left[\mathbf{K}_{\phi u}\right]_{\mathrm{s}} \dot{\mathbf{d}}_{\mathrm{s}}. \end{aligned} \tag{51}$$

Substituting equations (50) and (51) into equation (48), we get

$$\mathbf{M}\ddot{\mathbf{d}} + \mathbf{C}\dot{\mathbf{d}} + \mathbf{K}^{*}\mathbf{d} = \mathbf{F} \tag{52}$$

where

$$\mathbf{K}^{*} = \mathbf{K}_{uu} + G_{\mathrm{d}} \left[\mathbf{K}_{u\phi}\right]_{\mathrm{s}} \left[\mathbf{K}_{\phi\phi}^{-1}\right]_{\mathrm{s}} \left[\mathbf{K}_{\phi u}\right]_{\mathrm{s}} \tag{53}$$

and $\mathbf{C}$ is the active damping matrix computed by

$$\mathbf{C} = G_{\mathrm{v}} \left[\mathbf{K}_{u\phi}\right]_{\mathrm{a}} \left[\mathbf{K}_{\phi\phi}^{-1}\right]_{\mathrm{s}} \left[\mathbf{K}_{\phi u}\right]_{\mathrm{s}}. \tag{54}$$

Table 1. Material properties of the piezoelectric and composites.

Property	PVDF	PZT-4	PZT-G1195N	T300/979	Gr/Ep
		Elastic properties			
E_{11} (GPa)	2	81.3	63	150	132.38
E_{22} (GPa)	2	81.3	63	9	10.76
E_{33} (GPa)	2	64.5	63	9	10.76
G_{12} (GPa)	1	30.6	24.2	7.1	3.61
G_{13} (GPa)	1	25.6	24.2	7.1	5.65
G_{23} (GPa)	1	25.6	24.2	2.5	5.65
ν_{11}	0.29	0.33	0.3	0.3	0.24
ν_{23}	0.29	0.43	0.3	0.3	0.24
ν_{13}	0.29	0.43	0.3	0.3	0.49
		Mass density			
ρ (kg m^{-3})	1800	7600	7600	1600	1578
		Piezoelectric coefficients			
d_{31} (m V^{-1})	0.046	-1.22×10^{-10}	254×10^{-12}	—	—
d_{32} (m V^{-1})	0.046	-1.22×10^{-10}	254×10^{-12}	—	—
		Electric permittivity			
p_{11} (F m^{-1})	0.1062×10^{-9}	1475	15.3×10^{-9}	—	—
p_{22} (F m^{-1})	0.1062×10^{-9}	1475	15.3×10^{-9}	—	—
p_{33} (F m^{-1})	0.1062×10^{-9}	1300	15×10^{-9}	—	—

If the structural damping effect is considered in equation (52), it can be rewritten

$$\mathbf{M}\ddot{\mathbf{d}} + (\mathbf{C} + \mathbf{C}_{\mathrm{R}})\,\dot{\mathbf{d}} + \mathbf{K}^{*}\mathbf{d} = \mathbf{F} \tag{55}$$

where $\mathbf{C}_{\mathrm{R}}$ is the Rayleigh damping matrix assumed to be a linear combination of $\mathbf{M}$ and $\mathbf{K}_{uu}$,

$$\mathbf{C}_{\mathrm{R}} = \alpha\mathbf{M} + \beta\mathbf{K}_{uu}, \tag{56}$$

in which α and β are the Rayleigh damping coefficients.

For static analysis, equation (52) is reduced to

$$\mathbf{K}^{*}\mathbf{d} = \mathbf{F}. \tag{57}$$

4. Numerical results

In this section, various numerical examples are given to show the accuracy and stability of the CS-FEM-DSG3 compared to some other published methods. We first demonstrate the accuracy of the CS-FEM-DSG3 solution in comparison with other available numerical results for the static and free vibration problems. We then show the performance of the present method for dynamic control of a plate integrated with piezoelectric sensors and actuators. Here, the properties of the piezoelectric composite plates, including elastic properties, mass density, piezoelectric coefficients and electric permittivity are given in table 1.

4.1. Free vibration analysis of a piezoelectric composite plate

In this section, we investigate the accuracy and efficiency of the CS-FEM-DSG3 element for analyzing natural frequencies of piezoelectric composite plates. We now consider a square five-ply piezoelectric laminated composite plate [p/0/90/0/p] in which p is denoted as a piezoelectric layer as shown in figure 7(a). The plate is simply supported and the ratio of thickness of each composite ply to the length is $t/a = 1/50$. The laminate configuration includes three layers of graphite/epoxy (Gp/Ep) with fiber orientations of [0/90/0]. Two continuous PZT-4 piezoelectric layers of thickness $0.1t$ are bonded to the upper and lower surfaces of the laminate. Two sets of electric boundary conditions are considered for the inner surfaces of the piezoelectric layers including (1) a closed-circuit condition in which the electric potential is kept at zero (grounded), and (2) an open-circuit condition in which the electric potential remains free (zero electric displacements). A non-dimensional $\bar{f} = f_1 a^2/(10\,000t\sqrt{\rho})$ is used.

Table 2. Non-dimensional natural frequency of the simply supported square piezoelectric composite plate [p/0/90/0/p].

	$\bar{f} = f_1 a^2/\left(10\,000t\sqrt{\rho}\right)$	
Method	Closed circuit	Open circuit
CS-FEM-DSG3	234.500	249.942
DSG3	229.390	252.900
FEM layerwise [7]	234.533	256.765
Q9—HSDT (11 dofs) [16]	230.461	250.597
Q9—FSDT (5 dofs) [16]	206.304	245.349
Analytical solution [19]	245.941	245.942

Table 2 shows the result for the first non-dimensional frequency of the piezoelectric composite plate with a uniform discretization 12 × 12, as shown in figure 7(b). In this study, the CS-FEM-DSG3 and DSG3 used the first-order shear deformation theory (FSDT) with only 5 degrees of freedom (dofs) per node while [7] used the layerwise theory and [16] used high-order shear deformation theory (HSDT)

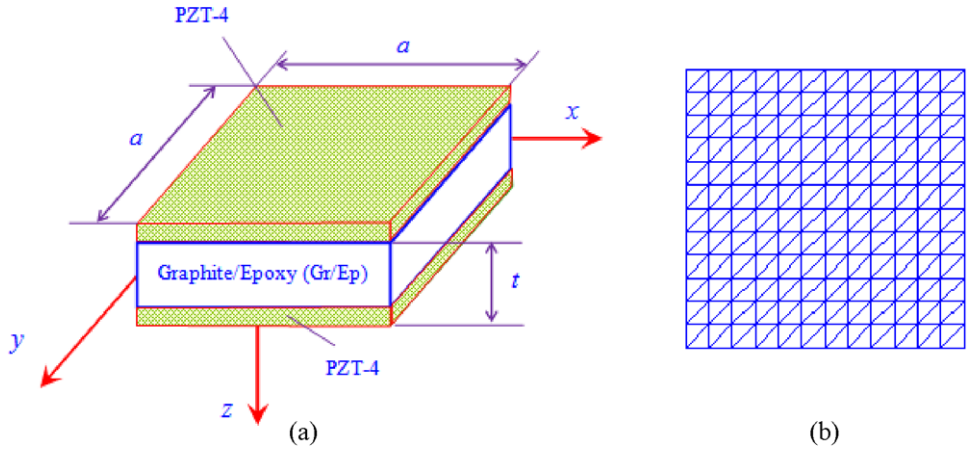

Figure 7. (a) The square piezoelectric composite plate model; (b) a discretization using triangular elements.

Table 3. Static deflection of the piezoelectric bimorph beam ($\times 10^{-6}$ m).

	Position				
Method	1	2	3	4	5
CS-FEM-DSG3	0.0139	0.0553	0.1243	0.2209	0.3451
DSG3	0.0142	0.0554	0.1244	0.2210	0.3452
EFG [20]	0.0142	0.0555	0.1153	0.2180	0.3416
3D FEM [23]	0.0136	0.0546	0.1232	0.2193	0.3410
RPIM [26]	0.0136	0.0547	0.1234	0.2196	0.3435
Analytical solution [17]	0.0140	0.0552	0.1224	0.2208	0.3451

with 11 dofs per node. It is seen that the results by the CS-FEM-DSG3 match well with the analytical solution [19] and agree very well with those by [7, 16]. In addition, the results by the CS-FEM-DSG3 are also much better than those by the DSG3.

Figure 8 plots the shapes of the first six lowest eigenmodes. It is seen that the shapes of the eigenmodes reflect correctly the real physical modes of the piezoelectric composite plate.

4.2. Static analysis

4.2.1. Piezoelectric bimorph beam. We now consider a bimorph piezoelectric beam with the geometry, thickness and boundary conditions illustrated in figure 9. The beam consists of identical PVDF uniaxial beams with opposite polarities. The cantilever beam is modeled by five identical plate elements. Each element has dimensions of 20 mm × 5 mm × 1 mm as shown in figure 9. The material properties of PVDF are shown in table 1.

Table 3 displays the deflections of the piezoelectric bimorph beam at the specified nodes when a unit voltage (1 V) is applied across the thickness of the beam. It is seen that the results by the CS-FEM-DSG3 match well with the analytical solution [17] and agree very well with those presented in [20, 23, 26]. In addition, the results by the CS-FEM-DSG3 are also better than those by the DSG3.

Next, table 4 shows the tip deflection of the piezoelectric bimorph beam with different input voltages. Again, it is seen that the results by the CS-FEM-DSG3 match well with the analytical solution [17] and are better than those by the DSG3. Lastly, figure 10 shows the effect of different input voltages on the deflection of the piezoelectric bimorph beam. It is observed that when the input voltage becomes larger, the deflection of the beam also becomes larger, as expected.

Table 4. Tip deflection of the piezoelectric bimorph beam with different input voltages ($\times 10^{-4}$ m).

	Input voltage			
Method	50 V	100 V	150 V	200 V
CS-FEM-DSG3	0.1726	0.3451	0.5177	0.6903
DSG3	0.1727	0.3452	0.5278	0.6904
Analytical solution [17]	0.1725	0.3451	0.5175	0.6900

4.2.2. Piezoelectric composite plate. We now consider a simply supported square laminate plate (20 cm × 20 cm) subjected to a uniform load $q = 100$ N m^{-2}. The plate is bonded by piezoelectric ceramics on both the upper and lower surfaces symmetrically. The plate consists of four composite layers and two outer piezo-layers denoted by p. The laminate configuration of the composite plate is $[\mathrm{p}/-\theta/\theta]_{\mathrm{s}}$ and $[\mathrm{p}/-\theta/\theta]_{\mathrm{as}}$ in which the subscripts 's' and 'as' indicate symmetric and antisymmetric laminates, respectively, and θ is the fiber orientation angle of the composite plate. The total thickness of the non-piezoelectric composite plate is 1 mm and each layer has the same thickness; the thickness of the piezo-layer is 0.1 mm. The plate is made of T300/976

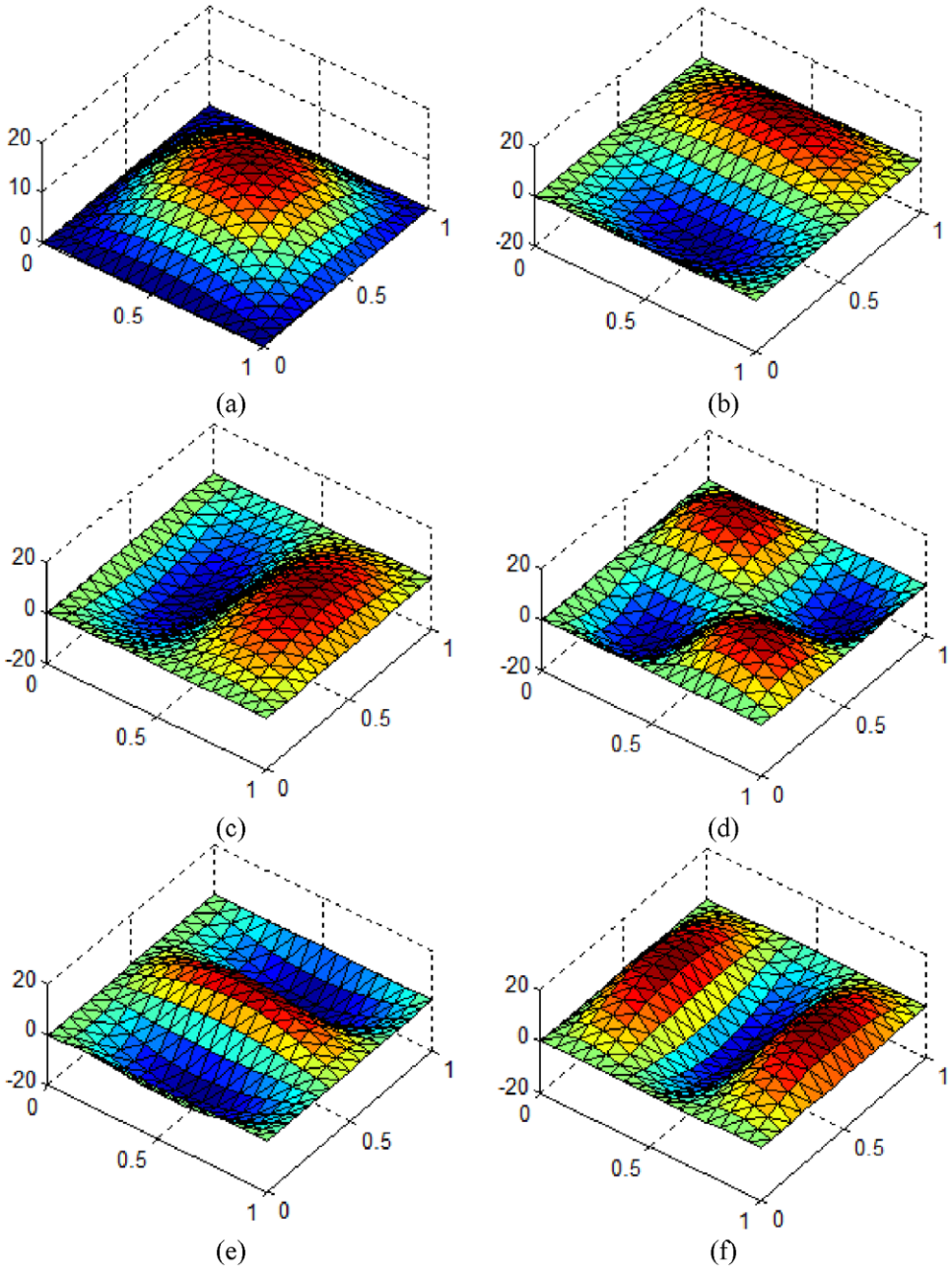

Figure 8. Shapes of the first six lowest eigenmodes of the simply supported piezoelectric composite plate by the CS-FEM-DSG3: (a) mode 1; (b) mode 2; (c) mode 3; (d) mode 4; (e) mode 5; (f) mode 6.

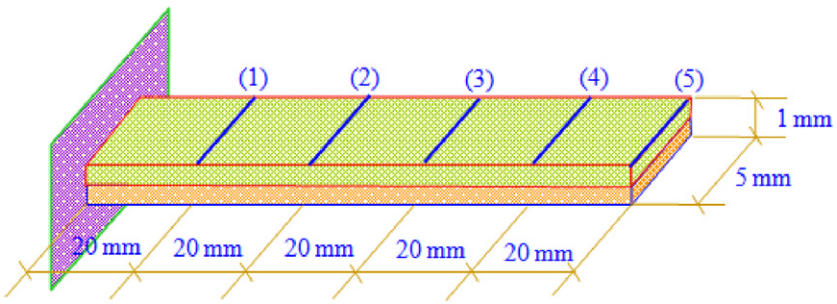

Figure 9. Geometry of a piezoelectric PVDF bimorph beam.

Table 5. Central node deflection of the simply supported piezoelectric composite plate subjected to a uniform load and different input voltages ($\times 10^{-4}$ m).

		Method		
Input voltage (V)	Scheme layer	CS-FEM-DSG3	DSG3	RPIM [26]
0	$[p/-45/45]_s$	−0.632 6	−0.511 6	−0.6038
	$[p/-45/45]_{as}$	−0.632 3	−0.530 8	−0.6217
	$[p/-30/30]_{as}$	−0.668 8	−0.560 3	−0.6542
	$[p/-15/15]_{as}$	−0.744 2	−0.622 9	−0.7222
5	$[p/-45/45]_s$	−0.286 3	−0.215 6	−0.2717
	$[p/-45/45]_{as}$	−0.280 1	−0.235 2	−0.2717
	$[p/-30/30]_{as}$	−0.295 7	−0.247 3	−0.2862
	$[p/-15/15]_{as}$	−0.325 9	−0.272 8	−0.3134
10	$[p/-45/45]_s$	0.060 04	0.080 41	0.0604
	$[p/-45/45]_{as}$	0.072 12	0.060 32	0.0757
	$[p/-30/30]_{as}$	0.077 42	0.065 64	0.0819
	$[p/-15/15]_{as}$	0.092 43	0.077 00	0.0954

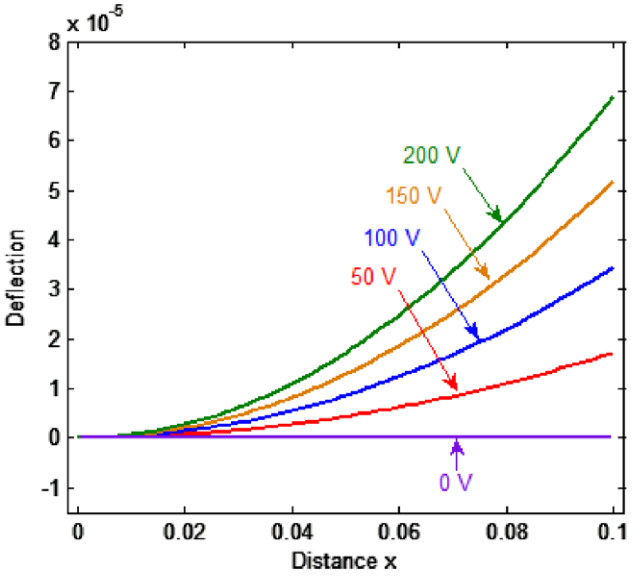

Figure 10. Centerline deflection of the piezoelectric bimorph beam under different input voltages.

graphite/epoxy layers and the piezoceramic is PZTG1195N with its material properties given in table 1.

Table 5 displays the central node deflection of the simply supported piezoelectric composite plate subjected to a uniform load and different input voltages with a uniform discretization 12 × 12. Again, it is seen that the results by the CS-FEM-DSG3 agree well with those by the RPIM [26] and show remarkably excellent performance compared to those by the DSG3. In addition, figure 11 shows the centerline deflection of the simply supported piezoelectric composite plate subjected to a uniform load and different input voltages. Four groups of different fiber orientation angles of the composite plate are investigated including $[p/-15/15]_{as}$, $[p/-30/30]_{as}$, $[p/-45/45]_{as}$ and $[p/-45/45]_s$. It is seen that when the input voltage becomes higher, the deflection becomes smaller, as expected. This is because when the input voltage is applied, it causes the piezoelectric effect and makes the plate deflect upward. This phenomenon, which is quite similar to that in the RPIM [26], can be seen clearly when an input voltage of 10 V is applied.

Next, we study the effect of the input voltage on the stress profile through the thickness of the symmetric and antisymmetric laminates as shown in figures 12–14. It can be seen that the stresses are discontinuous at the surface of layers of the laminate plate, as expected. Especially in the case of antisymmetric laminates, the stresses are discontinuous at the center position of the plate along the thickness direction as shown in figures 12(b), 13(b) and 14(b). In addition, it can be observed that when a higher input voltage is applied, it causes a stronger piezoelectric effect on the stresses induced in the plate. Specifically, it reduces the stress σ_x significantly as shown in figure 12 and even inverses the stress σ_{xy} as shown in figure 13.

Lastly, we analyze the effect of the number of composite layers on the stress profile through the thickness of the simply supported piezoelectric composite plate, as shown in figure 15. It is seen that when the number of layers in the laminate plate becomes smaller, the stress becomes larger. This is because when the laminate plate has more layers, each layer will share the stress together (the discontinuous line at the interface between the layers). Therefore, the stress decreases when the number of layers increases, as expected.

In summary, the results of the numerical examples in this section illustrate the expected static performance of the piezoelectric composite plates. The results by the CS-FEM-DSG3 agree well with the reference solutions and are better than those by the DSG3. This is because the gradient smoothing technique used in the CS-FEM-DSG3 can help to soften the over-stiff behavior in the DSG3, and hence improves the accuracy of the numerical results significantly.

4.3. Dynamic vibration control analysis of a piezoelectric composite plate

We now consider a piezoelectric composite plate with geometry, boundary conditions and material properties the same as those in section 4.2.2. The plate consists of four composite layers and two outer piezo-layers denoted by p. The upper and lower surfaces of the plate are made of a

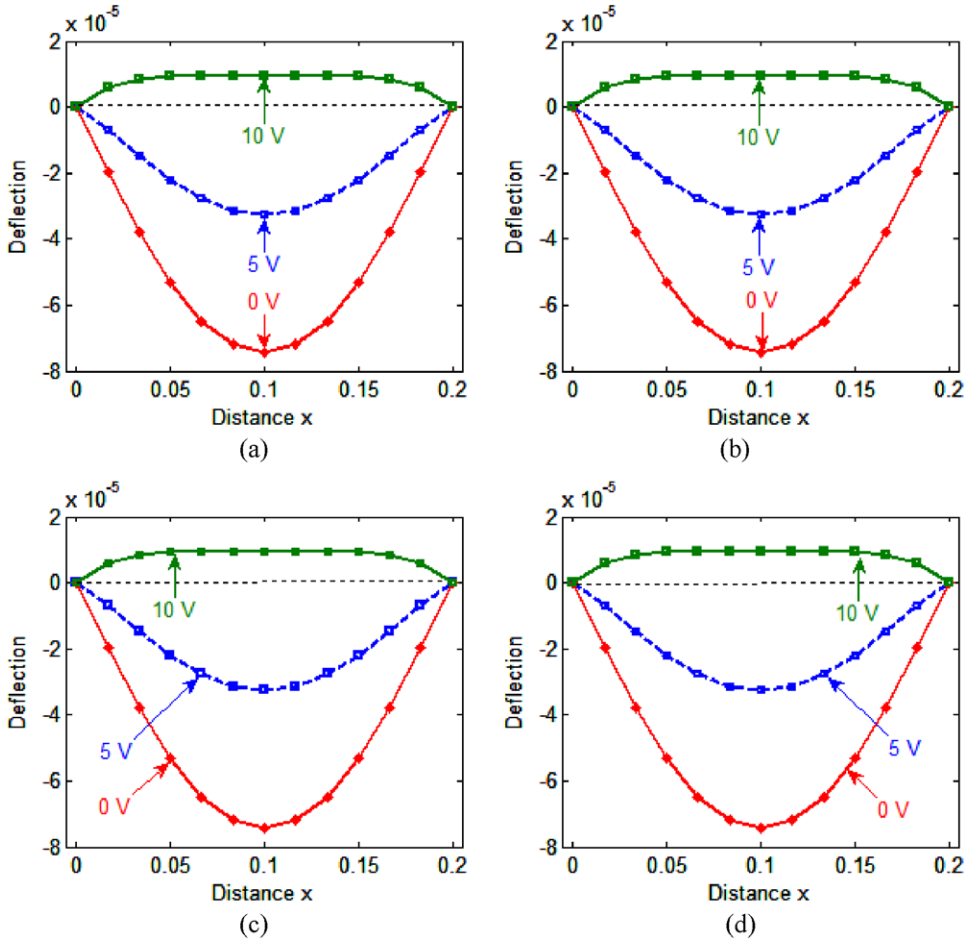

Figure 11. Centerline deflection of the simply supported piezoelectric composite plate subjected a uniform load and different input voltages. (a) $[p/–15/15]_{as}$. (b) $[p/–30/30]_{as}$. (c) $[p/–45/45]_{as}$. (d) $[p/–45/45]_{s}$.

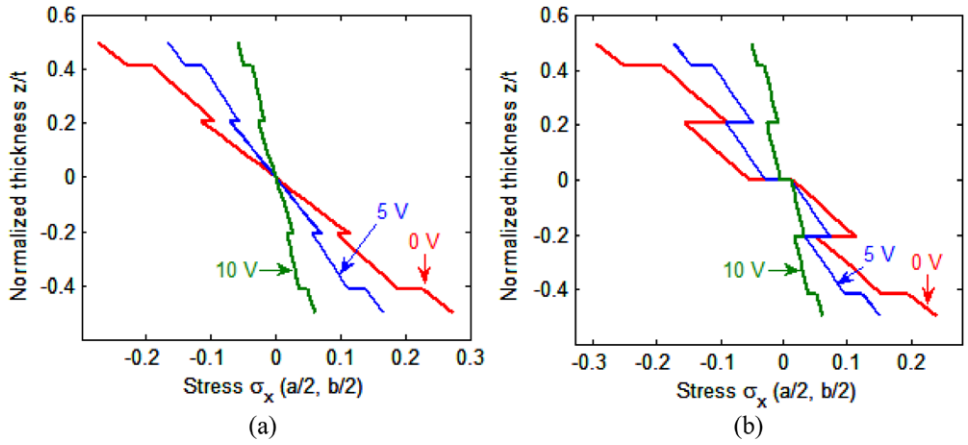

Figure 12. The stress profile σ_x through the thickness of a simply supported piezoelectric composite plate subjected to a uniform load and different input voltages. (a) $[p/–45/45]_{s}$. (b) $[p/–45/45]_{as}$.

piezoelectric actuator and a piezoelectric sensor. The stacking sequence of the composite plate is $[p/–45/45]_{s}$.

First, we study the control of the static deflection. Figure 16 shows the effect of the displacement feedback control gain G_d on the static deflection of a simply supported piezoelectric composite plate subjected to a uniform load. It is seen that when the displacement feedback control gain G_d becomes larger, the deflection becomes smaller, as expected. This phenomenon is quite similar to that in the RPIM [26]. This is because when the plate is deformed by an external force, electric charges are generated in the sensor layer and are amplified through closed loop control to convert into the

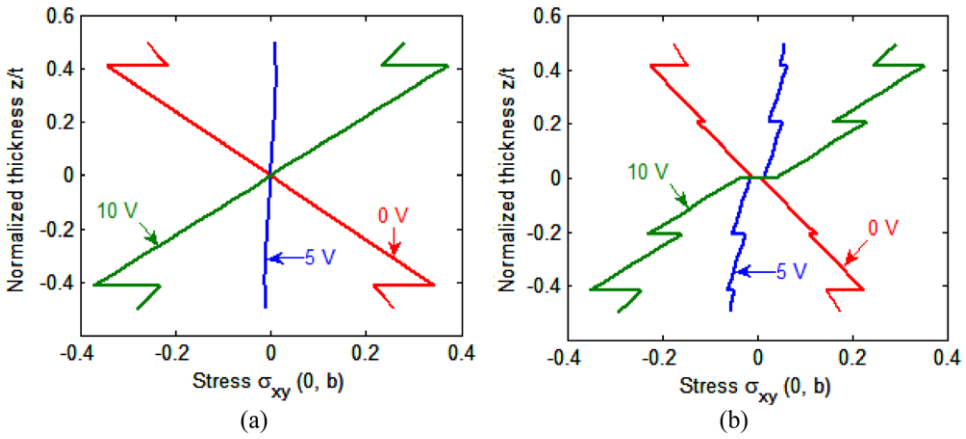

Figure 13. The stress profile σ_{xy} through the thickness of a simply supported piezoelectric composite plate subjected to a uniform load and different input voltages. (a) $[p/–45/45]_s$. (b) $[p/–45/45]_{as}$.

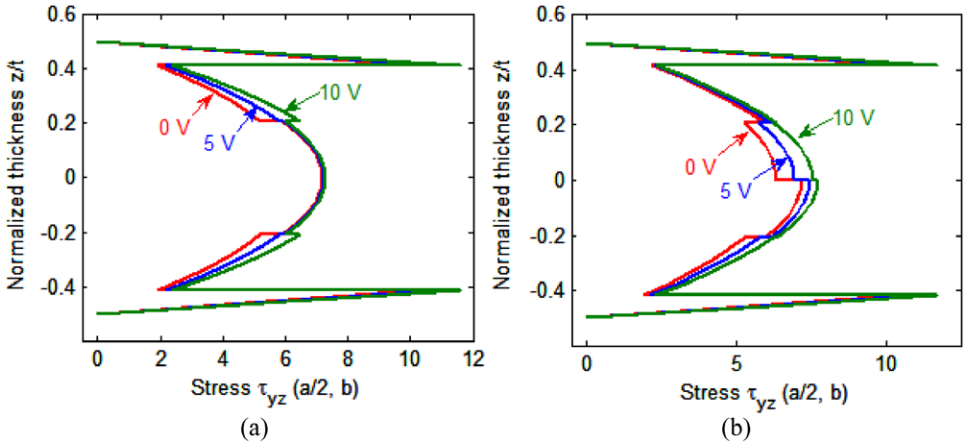

Figure 14. The stress profile τ_{yz} through the thickness of a simply supported piezoelectric composite plate subjected to a uniform load and different input voltages. (a) $[p/–45/45]_s$. (b) $[p/–45/45]_{as}$.

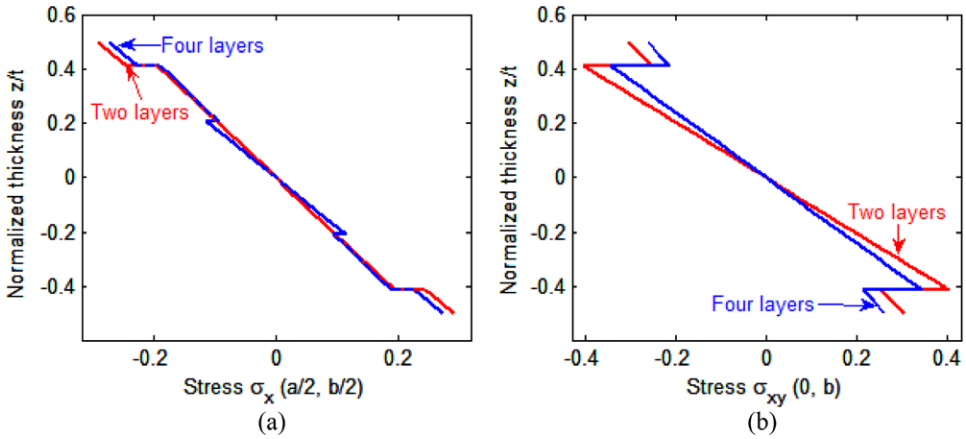

Figure 15. Effect of number of layers of composite on the stress profile through the thickness of a simply supported piezoelectric composite plate: (a) σ_x; (b) σ_{xy}.

signal. The converted signal is then sent to the distributed actuator and an input voltage for the actuators is generated through the converse piezoelectric effect. Finally, a resultant force is formed to actively control the static response of the laminate plate.

Next, figure 17 shows the transient response of the center point of the piezoelectric composite plate by using the velocity feedback gain. It can be seen that when the gain G_v equals zero (without control), the response decreases with respect to time due to the structural damping. In addition, by increasing

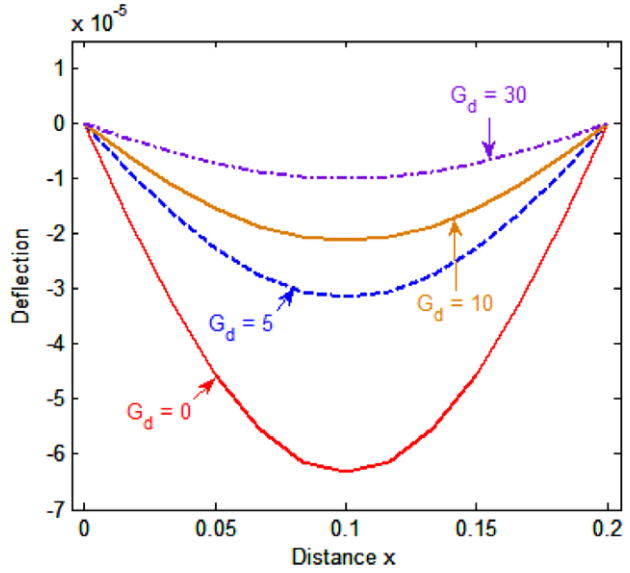

Figure 16. Effect of the displacement feedback control gain G_d on the static deflection of a simply supported piezoelectric composite plate subjected to a uniform load.

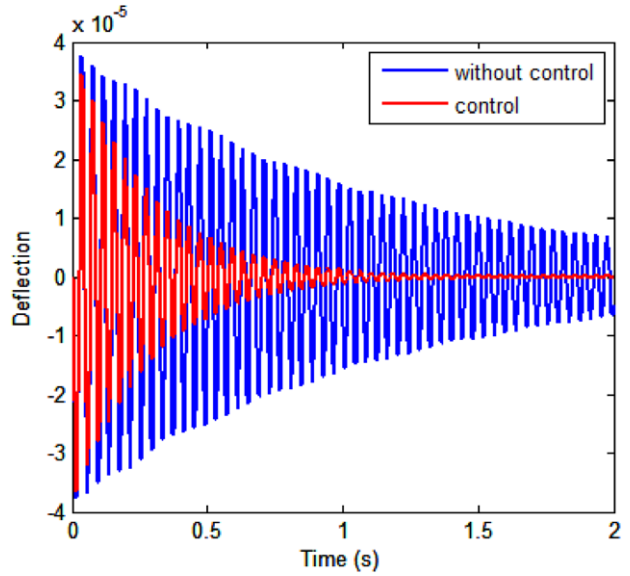

Figure 17. Effect of the velocity feedback control gain G_v on the dynamic response of deflection of a simply supported piezoelectric composite plate subjected to a uniform load.

the velocity feedback gain, the transient response is further suppressed and the amplitude of deflection of the center point of the plate decreases faster, as expected. This is because the active damping becomes stronger, as shown in equation (55).

5. Conclusions

The paper presents an extension of the CS-FEM-DSG3 to static and free vibration analyses and dynamic control of composite plates integrated with piezoelectric sensors and actuators. In the piezoelectric composite plates, the electric potential is assumed to be a linear function through the thickness for each piezoelectric sublayer. A displacement and velocity feedback control algorithm was used to adjust the static deflection as well as for active vibration control. Several numerical examples are given to analyze the static deflection, natural vibration mode and dynamic control of piezoelectric laminated plates with different stacking schemes. From the present formulation and numerical results, we can make the following points.

(i) The present CS-FEM-DSG3 only uses three-node triangular elements that are very easily generated automatically for complicated geometry domains.

(ii) The CS-FEM-DSG3 uses only five degrees of freedom at each vertex node. The CS-FEM-DSG3 is free of shear locking for piezoelectric laminated composite plates.

(iii) Due to using the gradient smoothing technique which can help to soften the over-stiff behavior in the DSG3, the proposed CS-FEM-DSG3 improves the accuracy of the numerical results significantly.

(iv) Although the present CS-FEM-DSG3 only uses the first-order shear deformation theory (FSDT), it still gives results which agree well with those using the layerwise theory and higher-order shear deformation theory (HSDT) for analysis of piezoelectric composite plates.

Acknowledgments

This work was supported by the Vietnam National Foundation for Science and Technology Development (NAFOSTED), Ministry of Science and Technology, under the basic research program (Project No. 107.02-2012.05).

References

[1] Wang Z, Chen S and Han W 1997 The static shape control for intelligent structures *Finite Elem. Anal. Des.* **26** 303–14
[2] Yang S M and Lee Y J 1994 Interaction of structure vibration and piezoelectric actuation *Smart Mater. Struct.* **3** 494–500
[3] Pletner B and Abramovich H 1997 Consistent methodology for the modelling of piezolaminated shells *AIAA J.* **35** 1316–26
[4] Hong C H and Chopra I 1999 Modeling and validation of induced strain actuation of composite coupled plates *AIAA J.* **37** 372–7
[5] Kim J, Varadan V V, Varadan V K and Bao X Q 1996 Finite element modeling of a smart cantilever plate and comparison with experiments *Smart Mater. Struct.* **5** 165–70
[6] Lam K Y, Peng X Q, Liu G R and Reddy J N 1997 A finite-element model for piezoelectric composite laminates *Smart Mater. Struct.* **6** 583–91
[7] Saravanos D A, Heyliger P R and Hopkins D A 1997 Layerwise mechanics and finite element for the dynamic analysis of piezoelectric composite plates *Int. J. Solids Struct.* **34** 359–78
[8] Wang S Y and Quek S T 2002 A model for the analysis of beams with embedded piezoelectric layers *J. Intell. Mater. Syst. Struct.* **13** 61–70
[9] Benjeddou A 2000 Advances in piezoelectric finite element modeling of adaptive structural elements: a survey *Comput. Struct.* **76** 347–63

[10] Allik H and Hughes T J R 1970 Finite element method for piezo-electric vibration *Int. J. Numer. Methods Eng.* **2** 151–7

[11] Kekana K 2002 Finite element modeling of laminated piezo-elastic structures: Lypunov stability analysis *J. Sound Vib.* **256** 463–73

[12] Wang S Y 2004 A finite element model for the static and dynamic analysis of a piezoelectric bimorph *Int. J. Solids Struct.* **41** 4075–96

[13] Cheng D K 1989 *Field and Wave Electromagnetics* 2nd edn (Reading, MA: Addison-Wesley)

[14] Ehlers S M and Weisshaar T A 1990 Static aeroelastic behavior of an adaptive laminated piezoelectric composite wing *AIAA J.* **28** 1611–23

[15] Wang S Y, Quek S T and Ang K K 2001 Vibration control of smart piezoelectric composite plates *Smart Mater. Struct.* **10** 637–44

[16] Victor M F C, Maria A A G, Afzal S, Cristóvão M M S, Carlos A M S and Franco C V M 2000 Modelling and design of adaptive composite structures *Comput. Methods Appl. Mech. Eng.* **185** 325–46

[17] Suleman A and Venkayya V B 1995 A simple finite element formulation for a laminated composite plate with piezoelectric layers *J. Intell. Mater. Syst. Struct.* **6** 776–682

[18] Chandrashekhara K and Agarwal A N 1993 Active vibration control of laminated composite plates using piezoelectric devices—a finite element approach *J. Intell. Mater. Syst. Struct.* **4** 496–508

[19] Heyliger P and Saravanos D A 1995 Exact free-vibration analysis of laminated plates with embedded piezoelectric layers *J. Acoust. Soc. Am.* **98** 1547–57

[20] Liew K M, Lim H K, Tan M J and He X Q 2002 Analysis of laminated composite beams and plates with piezoelectric patches using the element free Galerkin method *Comput. Mech.* **29** 486–97

[21] Bailey T and Hubbard J E 1985 Distributed piezoelectric-polymer active control of a cantilever beam *J. Guid. Control Dyn.* **8** 605–11

[22] Shen I Y 1995 Bending and torsional vibration control of composite beams through intelligent constrained-layer damping treatments *Smart Mater. Struct.* **4** 340–55

[23] Tzou H S and Tseng C I 1990 Distributed piezoelectric sensor/actuation design for dynamic measurement/control of distributed systems: an piezoelectric finite element approach *J. Sound Vib.* **138** 17–34

[24] Kapuria S and Yasin M Y 2013 Active vibration control of smart plates using directional actuation and sensing capability of piezoelectric composites *Acta Mech.* **224** 1185–99

[25] Hwang W S and Park H C 1993 Finite element modeling of piezoelectric sensors and actuators *AIAA J.* **31** 930–7

[26] Liu G R, Dai K Y and Lim K M 2004 Static and vibration control of composite laminates integrated with piezoelectric sensors and actuators using the radial point interpolation method *Smart Mater. Struct.* **13** 1438–47

[27] Liu G R, Peng X Q, Lam K Y and Tani J 1999 Vibration control simulation of laminated composite plates with integrated piezoelectrics *J. Sound Vib.* **220** 827–46

[28] Milazzo A and Orlando C 2012 An equivalent single-layer approach for free vibration analysis of smart laminated thick composite plates *Smart Mater. Struct.* **21** 075031

[29] Khdeir A A and Aldraihem O J 2011 Analysis of smart cross ply laminated shells with shear piezoelectric actuators *Smart Mater. Struct.* **20** 105030

[30] Raja S, Sinha P K, Prathap G and Dwarakanathan D 2004 Influence of active stiffening on dynamic behaviour of piezo-hygrothermo-elastic composite plates and shells *J. Sound Vib.* **278** 257–83

[31] Chen J S, Wu C T, Yoon S and You Y 2001 A stabilized conforming nodal integration for Galerkin mesh-free methods *Int. J. Numer. Methods Eng.* **50** 435–66

[32] Liu G R and Nguyen Thoi T 2010 *Smoothed Finite Element Methods* (New York: CRC Press)

[33] Liu G R, Dai K Y and Nguyen-Thoi T 2007 A smoothed finite element for mechanics problems *Comput. Mech.* **39** 859–77

[34] Nguyen-Thoi T, Liu G R, Dai K Y and Lam K Y 2007 Selective smoothed finite element method *Tsinghua Sci. Technol.* **12** 497–508

[35] Dai K Y, Liu G R and Nguyen-Thoi T 2007 An *n*-sided polygonal smoothed finite element method (nSFEM) for solid mechanics *Finite Elem. Anal. Des.* **43** 847–60

[36] Liu G R, Nguyen-Thoi T, Nguyen-Xuan H, Dai K Y and Lam K Y 2009 On the essence and the evaluation of the shape functions for the smoothed finite element method (SFEM) (Letter to Editor)c *Int. J. Numer. Methods Eng.* **77** 1863–9

[37] Liu G R, Nguyen-Thoi T, Nguyen-Xuan H and Lam K Y 2009 A node-based smoothed finite element method (NS-FEM) for upper bound solutions to solid mechanics problems *Comput. Struct.* **87** 14–26

[38] Nguyen-Thoi T, Liu G R, Nguyen-Xuan H and Nguyen-Tran C 2011 Adaptive analysis using the node-based smoothed finite element method (NS-FEM) *Commun. Numer. Methods Eng.* **27** 198–218

[39] Nguyen-Thoi T, Liu G R and Nguyen-Xuan H 2009 Additional properties of the node-based smoothed finite element method (NS-FEM) for solid mechanics problems *Int. J. Comput. Methods* **6** 633–66

[40] Liu G R, Nguyen-Thoi T and Lam K Y 2009 An edge-based smoothed finite element method (ES-FEM) for static and dynamic problems of solid mechanics *J. Sound Vib.* **320** 1100–30

[41] Nguyen-Thoi T, Liu G R and Nguyen-Xuan H 2011 An *n*-sided polygonal edge-based smoothed finite element method (nES-FEM) for solid mechanics *Commun. Numer. Methods Eng.* **27** 1446–72

[42] Nguyen-Thoi T, Liu G R, Lam K Y and Zhang G Y 2009 A face-based smoothed finite element method (FS-FEM) for 3D linear and nonlinear solid mechanics problems using 4-node tetrahedral elements *Int. J. Numer. Methods Eng.* **78** 324–53

[43] Liu G R, Nguyen-Thoi T and Lam K Y 2008 A novel alpha finite element method (αFEM) for exact solution to mechanics problems using triangular and tetrahedral elements *Comput. Methods Appl. Mech. Eng.* **197** 3883–97

[44] Liu G R, Nguyen-Thoi T and Lam K Y 2009 A novel FEM by scaling the gradient of strains with factor α (αFEM) *Comput. Mech.* **43** 369–91

[45] Liu G R, Nguyen-Xuan H, Nguyen-Thoi T and Xu X 2009 A novel Galerkin-like weakform and a superconvergent alpha finite element method (SαFEM) for mechanics problems using triangular meshes *J. Comput. Phys.* **228** 4055–87

[46] Liu G R, Nguyen-Xuan H and Nguyen-Thoi T 2011 A variationally consistent αFEM (VCαFEM) for solid mechanics problems *Int. J. Numer. Methods Eng.* **85** 461–97

[47] Liu G R, Nguyen-Thoi T, Dai K Y and Lam K Y 2007 Theoretical aspects of the smoothed finite element method (SFEM) *Int. J. Numer. Methods Eng.* **71** 902–30

[48] Liu G R, Nguyen-Xuan H and Nguyen-Thoi T 2010 A theoretical study on NS/ES-FEM: properties, accuracy and convergence rates *Int. J. Numer. Methods Eng.* **84** 1222–56

[49] Nguyen-Xuan H and Nguyen-Thoi T 2009 A stabilized smoothed finite element method for free vibration analysis of Mindlin–Reissner plates *Int. J. Numer. Methods Biomed. Eng.* **25** 882–906

[50] Cui X Y, Liu G R, Li G Y, Zhao X, Nguyen-Thoi T and Sun G Y 2008 A smoothed finite element method (SFEM) for linear and geometrically nonlinear analysis of plates and shells *Comput. Model. Eng. Sci.* **28** 109–25

[51] Nguyen-Thoi T, Phung-Van P, Luong-Van H, Nguyen-Van H and Nguyen-Xuan H 2013 A cell-based smoothed three-node Mindlin plate element (CS-MIN3) for static and free vibration analyses of plates *Comput. Mech.* **50** 65–81

[52] Nguyen-Thoi T, Bui-Xuan T, Phung-Van P, Nguyen-Xuan H and Ngo-Thanh P 2013 Static, free vibration and buckling analyses of stiffened plates by CS-FEM-DSG3 using triangular elements *Comput. Struct.* **125** 100–13

[53] Nguyen-Xuan H, Rabczuk T, Nguyen-Thanh N, Nguyen-Thoi T and Bordas S 2010 A node-based smoothed finite element method with stabilized discrete shear gap technique for analysis of Reissner–Mindlin plates *Comput. Mech.* **46** 679–701

[54] Nguyen-Xuan H, Loc T V, Chien T H and Nguyen-Thoi T 2012 Analysis of functionally graded plates by an efficient finite element method with node-based strain smoothing *Thin-Walled Struct.* **54** 1–18

[55] Thai-Hoang C, Tran-Vinh L, Tran-Trung D, Nguyen-Thoi T and Nguyen-Xuan H 2012 Analysis of laminated composite plates using higher-order shear deformation plate theory and node-based smoothed discrete shear gap method *Appl. Math. Modelling* **36** 5657–77

[56] Nguyen-Xuan H, Tran-Vinh L, Nguyen-Thoi T and Vu-Do H C 2011 Analysis of functionally graded plates using an edge-based smoothed finite element method *Compos. Struct.* **93** 3019–39

[57] Phung-Van P, Nguyen-Thoi T, Tran V L and Nguyen-Xuan H 2013 A cell-based smoothed discrete shear gap method (CS-DSG3) based on the C0-type higher-order shear deformation theory for static and free vibration analyses of functionally graded plates *Comput. Mater. Sci.* doi:10.1016/j.commatsci.2013.06.010

[58] Nguyen-Thoi T, Phung-Van P, Thai-Hoang C and Nguyen-Xuan H 2013 A cell-based smoothed discrete shear gap method (CS-DSG3) using triangular elements for static and free vibration analyses of shell structures *Int. J. Mech. Sci.* **74** 32–45

[59] Nguyen-Thoi T, Bui-Xuan T, Phung-Van P, Nguyen-Hoang S and Nguyen-Xuan H 2013 An edge-based smoothed three-node Mindlin plate element (ES-MIN3) for static and free vibration analyses of plates *KSCE J. Civ. Eng.* at press

[60] Phan-Dao H H, Nguyen-Xuan H, Thai-Hoang C, Nguyen-Thoi T and Rabczuk T 2013 An edge-based smoothed finite element method for analysis of laminated composite plates *Int. J. Comput. Methods* **10** 1340005

[61] Nguyen-Xuan H, Liu G R, Thai-Hoang C and Nguyen-Thoi T 2009 An edge-based smoothed finite element method with stabilized discrete shear gap technique for analysis of Reissner–Mindlin plates *Comput. Methods Appl. Mech. Eng.* **199** 471–89

[62] Nguyen-Xuan H, Liu G R, Nguyen-Thoi T and Nguyen-Tran C 2009 An edge-based smoothed finite element method (ES-FEM) for analysis of two-dimensional piezoelectric structures *Smart Mater. Struct.* **18** 1–12

[63] Liu G R, Chen L, Nguyen-Thoi T, Zeng K and Zhang G Y 2010 A novel singular node-based smoothed finite element method (NS-FEM) for upper bound solutions of cracks *Int. J. Numer. Methods Eng.* **83** 1466–97

[64] Nguyen-Thoi T, Liu G R, Vu-Do H C and Nguyen-Xuan H 2009 An edge-based smoothed finite element method (ES-FEM) for visco-elastoplastic analyses of 2D solids using triangular mesh *Comput. Mech.* **45** 23–44

[65] Nguyen-Thoi T, Vu-Do H C, Rabczuk T and Nguyen-Xuan H 2010 A node-based smoothed finite element method (NS-FEM) for upper bound solution to visco-elastoplastic analyses of solids using triangular and tetrahedral meshes *Comput. Methods Appl. Mech. Eng.* **199** 3005–27

[66] Nguyen-Thoi T, Liu G R, Vu-Do H C and Nguyen-Xuan H 2009 A face-based smoothed finite element method (FS-FEM) for visco-elastoplastic analyses of 3D solids using tetrahedral mesh *Comput. Methods Appl. Mech. Eng.* **198** 3479–98

[67] Nguyen-Xuan H, Rabczuk T, Nguyen-Thoi T, Tran T N and Nguyen-Thanh N 2012 Computation of limit and shakedown loads using a node-based smoothed finite element method *Int. J. Numer. Methods Eng.* **90** 287–310

[68] Le-Van C, Nguyen-Xuan H, Askes H, Rabczuk T and Nguyen-Thoi T 2013 Computation of limit load using edge-based smoothed finite element method and second-order cone programming *Int. J. Comput. Methods* **10** 1340005

[69] Tran T N, Liu G R, Nguyen-Xuan H and Nguyen-Thoi T 2010 An edge-based smoothed finite element method for primal–dual shakedown analysis of structures *Int. J. Numer. Methods Eng.* **82** 917–38

[70] Nguyen-Thoi T, Phung-Van P, Rabczuk T, Nguyen-Xuan H and Le-Van C 2013 Free and forced vibration analysis using the *n*-sided polygonal cell-based smoothed finite element method (*n*CS-FEM) *Int. J. Comput. Methods* **10** 1340008

[71] Chen L, Zhang G Y, Zhang J, Nguyen-Thoi T and Tang Q 2011 An adaptive edge-based smoothed point interpolation method for mechanics problems *Int. J. Comput. Math.* **88** 2379–402

[72] Wu S C, Liu G R, Cui X Y, Nguyen-Thoi T and Zhang G Y 2010 An edge-based smoothed point interpolation method (ES-PIM) for heat transfer analysis of rapid manufacturing system *Int. J. Heat Mass Transfer* **53** 1938–50

[73] Nguyen-Thoi T, Phung-Van P, Rabczuk T, Nguyen-Xuan H and Le-Van C 2013 An application of the ES-FEM in solid domain for dynamic analysis of 2D fluid–solid interaction problems *Int. J. Comput. Methods* **10** 1340003

[74] Nguyen-Thoi T, Phung-Van P, Nguyen-Xuan H and Thai-Hoang C 2012 A cell-based smoothed discrete shear gap method using triangular elements for static and free vibration analyses of Reissner–Mindlin plates *Int. J. Numer. Methods Eng.* **91** 705–41

[75] Bletzinger K U, Bischoff M and Ramm E 2000 A unified approach for shear-locking free triangular and rectangular shell finite elements *Comput. Struct.* **75** 321–34

[76] Reddy J N 1997 *Mechanics of Laminated Composite Plates—Theory and Analysis* (New York: CRC Press)

Queries for IOP paper 470236

Journal: **SMS**
Author: **P Phung-Van *et al***
Short title: **Static and free vibration analyses and dynamic control of composite plates integrated with piezoelectric sensors and actuators by the cell-based smoothed discrete shear gap method (CS-FEM-DSG3)**

Page 1

Query 1:
Author: Please check that the author names and affiliations as given are spelt correctly.

Page 1

Query 2:
Author: Please be aware that the colour figures in this article will only appear in colour in the Web version. If you require colour in the printed journal and have not previously arranged it, please contact the Production Editor now.

Page 1

Query 3:
Author: In several places (including the title) I have standardized the English somewhat. Please check that I have not inadvertently altered the meaning.

Page 2

Query 4:
Author: Please define 'FEM' here.

Page 2

Query 5:
Author: Can 'weakform' be changed to 'weak form' throughout? Please check.

Page 5

Query 6:
Author: Would the title to section 2.3.3.1 read better as 'Brief description of the ...'? Please check.

Page 8

Query 7:
Author: This sentence has been reworded for clarity. Please check that the meaning is still correct.

Page 12

Query 8:
Author: Please check 'Scheme layer' in table 5. Should this be 'Layer scheme'?

Page 12

Query 9:
Author: Please check 'surface of layers' here. Should this be 'surface layers'?

Page 12

Query 10:
Author: Please check 'inverses' here. Should this be 'reverses'?

Page 15

Query 11:
Author: This sentence has been reworded for clarity. Please check that the meaning is still correct.

Page 15

Query 12:
Author: Please check the details for any journal references that do not have a blue link as they may contain some incorrect information. Pale purple links are used for references to arXiv e-prints.

Page 15

Query 13:
Author: References [26, 29] in the author pdf have been deleted from the reference list since they were repetitions of references [6, 28]. Please check.

Page 16

Query 14:
Author: [17]: Please check the page range given.

Page 16

Query 15:
Author: [32]: Please check the second author name given.

Page 17

Query 16:
Author: [50, 54]: Please check the journal title given.

Page 17

Query 17:
Author: [54]: Please check the second and third author name given.

Page 17

Query 18:
Author: [55]: Please check the author names given.

Page 17

Query 19:
Author: [57]: Please provide volume and page/article number.

Page 17

Query 20:
Author: [59]: Any update?

Uncited References

Reference [65] is not cited in the text, either remove it from the reference list or cite.